PhD Degree in System Medicine
Curriculum in Human Genetics
European School of Molecular Medicine (SEMM),
University of Milan and University of Naples "Federico II"
Settore disciplinare:Bio/17

MiT/TFE factors control ER-phagy via transcriptional regulation of FAM134B

Maria Iavazzo

Telethon Institute of Genetics and Medicine (TIGEM)

Tutor: Prof. Carmine Settembre

TIGEM; Federico II University, Italy.

Internal Advisor: Prof. Paolo Grumati

TIGEM; Federico II University, Italy.

External Advisor: Prof. Fulvio Reggiori

University of Groningen, The Netherlands

PhD Coordinator: Prof. Saverio Minucci

Anno accademico 2021-2022

List of Abbreviations

ER: Endoplasmic reticulum

LIR or **GIM**: LC3 or GABARAP interaction motif

FGF: Fibroblast growth factor

PI3K: Phosphoinositide 3-kinases

mTOR: mechanistic target of rapamycin

TFEB: Transcription factor EB

TFE3: Transcription factor binding to IGHM Enhancer 3

AVs: autophagic vesicles

ARs: Autophagy receptors

RHD: reticulon homology domain

IM: intramembrane

TM: transmembrane

ERES: ER exit sites

FIR: FIP200 interacting region

CLEAR: coordinated lysosomal expression and regulation

mTORC1: mechanistic target of rapamycin complex 1

MCOLN1: Ca2+ channel mucolipin 1

FGFR: Fibroblast growth factor receptor

Table of Contents

Figures Index....3
Abstract....4
Introduction....5
The endoplasmic reticulum (ER)....6
Selective autophagy of the ER: ER-phagy....7
FAM134 family proteins....9
Transcriptional control of the ER-phagy pathway....10
TFEB and TFE3: Master regulator of autophagy and lysosome....11
Fibroblast growth factor signalling in the growth plate....13
Results....15
FGF signalling induces lysosome biogenesis and ER-phagy in chondrocytes....16
FGF18 inhibits the PI3K signalling cascade through FGFR3/4 receptors....18
FGF signalling activates ER-phagy via TFEB/TFE3-mediated FAM134B induction....24
FGF signalling induces ER-phagy in mice cartilage....28
Discussion....31
FGF mediate ER-phagy might promote chondrocytes differentiation....34
FAM134B mediated ER-phagy promotes misfolded collagen clearance....35
TFEB/TFE3 could promote bulk and different selective autophagy....35
Concluding Remarks....36
Materials and Methods....37
Cell culture, transfections, and plasmids....38
Plasmids....38
Generation of CRISPR clones....38
Transmission electron microscopy....39
EATR assay....39
GFP-mCherry-LC3 assay....39
Western blotting....40
Lysosomal enzymatic activity....40
LysoTracker and DQ-BSA experiments....40
qRT–PCR....41
QuantSeq 3’ mRNA sequencing library preparation....42
QuantSeq3’mRNA sequencing data processing and analysis....42
MS-proteomics and phospho-proteomics....42
MS data processing and analysis....43
Tandem mass tag secretome....43

Tandem mass tag secretome analysis 44
Chromatin immunoprecipitation (ChIP) 44
Luciferase assay 44
Mice 45
Cartilage and bone staining 45
References 46

Figures Index

Figure 1. Autophagy of the Endoplasmic Reticulum....8

Figure 2. Schematic overview of the mammalian ER-phagy receptors....9

Figure 3. The lysosome to nucleus signalling pathway of TFEB....12

Figure 4. FGF18 induces lysosome biogenesis in chondrocytes....16

Figure 5. FGF18 promotes lysosome catabolic activity in chondrocytes....17

Figure 6. FGF18 regulates ER-phagy in chondrocytes....18

Figure 7. FGF18 induces lysosome biogenesis and activity through FGFR3 and FGFR4....19

Figure 8 FGF18 induces lysosome biogenesis and ER-phagy through FGFR3 and FGFR4....20

Figure 9. FGF18 inhibits the insulin/PI3K pathway....21

Figure 10. FGF18 induces lysosome biogenesis and ER-phagy via a transcriptional control mechanism....22

Figure 11. FGF18 enhances *Fam134b* expression....23

Figure 12. FGF18 induces ER-phagy via FAM134B....24

Figure 13. FGF18 activates TFEB and TFE3 transcription factors....25

Figure 14. FGF signalling regulates *Fam134b* transcriptional levels through TFEB and TFE3....26

Figure 15. FGF18 induces *Fam134b-2* via TFEB activation in RCS....27

Figure 16. Fam134b-1 and Fam134b-2 rescued CLIMP63 lysosomal accumulation in Fam134bΔLIR cells....28

Figure 17. FGF signaling controls ER-phagy *in vivo*....29

Figure 18. FAM134B is required for protein secretion in RCS....30

Figure 19. Proposed model of induced ER-phagy in chondrocytes....32

Figure 20. FGF18 might promote chondrocytes differentiation....34

Abstract

Lysosomes are catabolic organelles devoted to the degradation of intracellular proteins and components. In addition, lysosomes are signalling hubs that orchestrate many intracellular responses. Lysosomal degradation of the endoplasmic reticulum (ER) via autophagy (ER-phagy) is emerging as a critical regulator of cell homeostasis and function. The recent identification of ER-phagy receptors has shed light on the molecular mechanisms underlining this process. ER-phagy receptors are ER membrane proteins or soluble proteins (such as CALCOCO1 and SQSTM1), that bind to cytosolic Atg8-family proteins via the LC3-Interacting Region (LIR) mediating the delivery of specific ER subdomains to lysosomes for degradation. Although the role of the ER-phagy in the regulation of ER size and cellular proteostasis has been well characterized, the upstream signalling pathway regulating ER-phagy in response to developmental and cellular needs is still largely unknown. Chondrocytes are highly secretory cells with an abundant ER, producing predominantly procollagen (PC) molecules in extracellular matrix during endochondral ossification. They reside in a poorly vascularized tissue, as the growth plate, with scarcity of nutrients, representing a good cellular model to study ER-phagy. We found that the nutrient responsive transcription factors TFEB and TFE3—master regulators of lysosomal biogenesis and autophagy—control ER-phagy by inducing the expression of the ER-phagy receptor FAM134B. The TFEB/TFE3-FAM134B axis is activated in chondrocytes by FGF signalling, a critical regulator of skeletal growth. We demonstrated that FGF18 induces lysosome biogenesis and ER-phagy in chondrocytes through the activation of FGFR3 and FGFR4 receptors, which in turn inhibit the PI3K/Akt-mTORC1 pathway and promote TFEB/TFE3 nuclear translocation and enhance *Fam134b* transcription. Notably, FAM134B is required for protein secretion in chondrocytes.

In conclusion, this study identifies a new signalling pathway that allows ER-phagy to respond to developmental cues suggesting potential therapeutic approaches for the treatment of skeletal features in multiple human diseases.

Introduction

Macroautophagy (hereafter referred as autophagy) is an evolutionarily conserved pathway devoted to the degradation of cytosolic constituents. Autophagy relies on the activity of two organelles, the autophagosomes (autophagic vesicles—AVs), which sequester substrates, and the lysosomes, where degradation occurs [1]. Initially described as non-specific, autophagy is now emerging as a selective process. Substrate selectivity in autophagy is mediated by the autophagy receptors (ARs) that recognize the cargo and drive the autophagosome formation around the cargo. ARs bring their LIR/GIM motifs, which stand for LC3 interacting region(s) and/or GABARAP-interaction motif(s), to interact with autophagosome-localizing ATG8 family-proteins [including LC3A, LC3B, LC3C, gamma-aminobutyric acid receptor-associated protein (GABARAP), gamma-aminobutyric acid receptor-associated protein-like (GABARAPL1, and GABARAPL2)] [2]. In the last years, the selective autophagy degradation of the endoplasmic reticulum (ER) into the lysosome, named as the ER-phagy, is significantly emerging [3]. ER-phagy has been involved in several functions, such as ER membrane remodelling, response to starvation, and cargo-quality control [4,5]. In the next sections will be deepened the ER-phagy mechanisms and the physiological role of ER-phagy mediated cargo degradation.

The endoplasmic reticulum (ER)

The ER, the largest organelle in the cell, is essential for a plethora of cellular functions including protein synthesis, transport and folding, lipid and steroid synthesis, carbohydrate metabolism and ion storage [5]. These functions occur in distinct domains consisting of tubules and sheets spreading from the nucleus to the plasma membrane [6]. Sheets and tubules are mostly connected through three-way junctions, which result in an ER having a cellular polygonal pattern [7]. The complexity of the ER structure has been further elucidated by ultra-structural studies. Super-resolution electron microscopy helped to identify membrane sheets as densely packed tubular arrays, also defined as ER matrix, which is important to many cellular functions (for instance ER matrix could form the nuclear envelope, helicoidal stacks in the perinuclear region, or flattened cisternal structures close to the plasma membrane) [8]. ER membranes are virtually divided into rough and smooth ER, although these membranes are functionally interconnected into gradients of functions [9]. The smooth ER is the site of lipids and steroid hormones biosynthesis, that furthermore acts as a hub for detoxification enzyme activity. The rough ER is decorated with ribosomes that are sites of transmembrane and secretory protein synthesis. Along with protein translation, ribosomes insert nascent polypeptide chains into the ER lumen and/or membrane.

Continuously, the ER needs to maintain high efficiency rates to dynamically adapt to cellular stress and the high demand of newly synthesized proteins [10]. During proteo-synthesis, newly synthesized polypeptides could exceptionally abort folding, inducing protein misfolding and aggregation, thus leading to ER Stress, cytotoxicity, and cell death [11;12]. Many human disorders, including neurodegenerative diseases, cataracts and atherosclerosis, late onset type 2 diabetes or ageing conditions are caused by alteration of ER fitness [13-15].

Selective autophagy of the ER: ER-phagy

The ER-phagy, literally endoplasmic reticulum (ER)-eating, was firstly observed in the 1950s by cell biology and electron microscopy pioneers [16]. The original micrographs reveal ER vesiculation and, at least, three different morphologically pathways to deliver ER portion to degradative compartment: 1) ER fragments captured by autophagosomes that eventually fuse with lysosomes (now named macro-ER-phagy); 2) ER fragments engulfed by degradative compartments (micro-ER-phagy); 3) fusion of ER vesicles with the degradative compartment (LC3-dependent vesicular delivery) (Figure 1). An increasing number of studies indicate that lysosomal ER clearance operates constitutively but is further enhanced by chemical stress and shortage of nutrients; during development or differentiation upon stimuli; by pharmacological treatment which causes ER enlargement/stress; in response to protein misfolding and/or retention [17]. The discovery of ER-phagy receptors has dramatically accelerated the characterization of constitutive and regulated ER turnover in eukaryotic cells. ER-phagy receptors share one or more LC3 interacting motif (LIR) or GABARAP-interacting motif (GIM), that facilitates binding of the cargo to autophagosomal LC3/GABARAP family proteins. LC3/GABARAP proteins decorate the autophagosome membrane, thus physically form a bridge between the ER fragments and autophagosomes [18].

The mammalian family of ER-phagy receptors includes (Figure 2): FAM134A, FAM134B-1, FAM134B-2, FAM134C, RTN3L, all characterized by two reticulon homology domain (RHD) [19-22]. The ER-phagy receptors that lack the RHD are: ATL3, SEC62, CCPG1, TEX264 [23-26]. FAM134B, RTN3L and ATL3 are proteins with an intramembrane (IM) region lacking an ER luminal domain and having function in shaping ER, modulating tubule/sheet ration and tubule branching [27-28]. RTN3 and ATL3 decorate ER tubules, whereas CCPG1, SEC62 and TEX264 are transmembrane (TM) proteins with a cytosolic ER-membrane and ER-luminal domains with no reported function in shaping ER membrane. Although transmembrane receptors are ubiquitous in the ER, TEX264 has been recently observed at three-way junctions suggesting that it might be enriched in these subdomains [29]. Notably, SEC62 is a subunit of the translocon complex, which controls translocation of

newly synthesized protein into the ER. The list of mammalians ER-phagy receptors also includes soluble receptors, such as CALCOCO1, C53, and SQSTM1. In addition, the cytosolic autophagy receptors NBR1 and OPTN can bind ubiquitinated ER-membrane proteins, suggesting that they are also involved in ER-turnover [30]. The role of ER-phagy receptors in the ER-phagy pathways is not completely understood therefore more efforts are needed to clarify how autophagy receptors demarcate and fragment the ER.

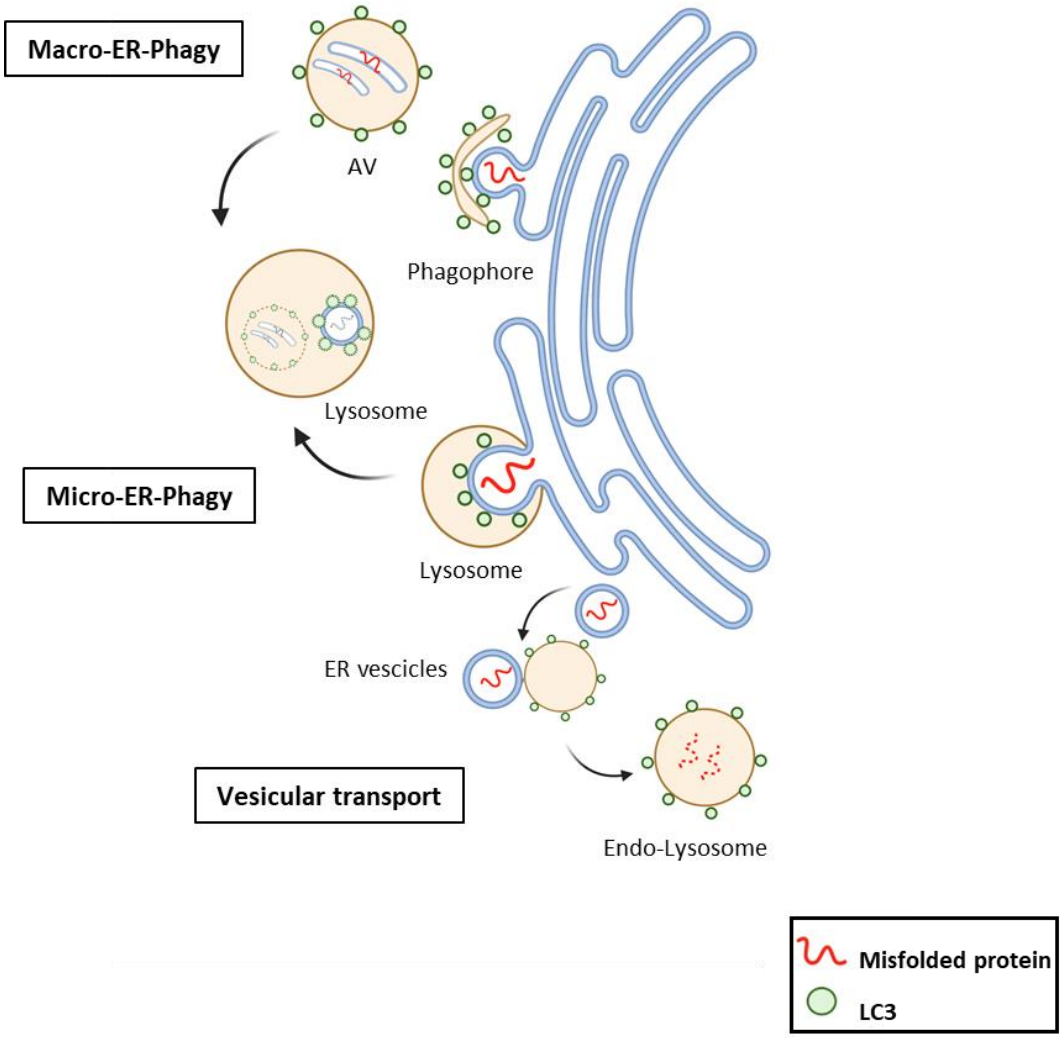

Figure 1. Autophagy of the Endoplasmic Reticulum (From top to bottom) **Macro-ER-phagy:** ER fragments are sequestered by double-membrane autophagosomes decorated with LC3 molecules (green dots). Autophagosomes then fuse with lysosomes for degradation. **Micro-ER-Phagy**: lysosomal invagination or protrusion directly engulfs ER exit sites (ERES) decorated with LC3. **Vesicular transport:** single membrane ER derived vesicles bud from the ER and fuse with lysosomes for degradation. Abbreviation: Endoplasmatic Reticulum (ER); Autophagic Vesicle (AV).

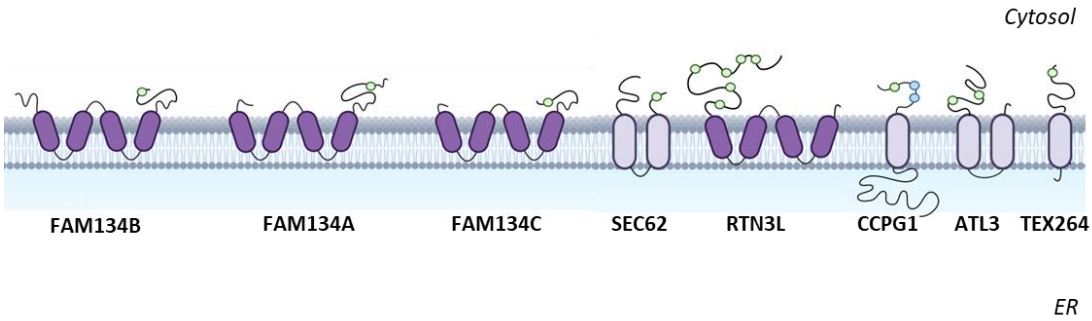

Figure 2. Schematic overview of the mammalian ER-phagy receptors Membrane-bound ER-phagy receptors in mammalian cells are depicted. Green dots represent LC3/GABARAP interacting region; Cerulean dots represent FIP200 interacting region (FIR).

FAM134 family proteins

The protein family with sequence similarity 134 (FAM134) includes three conserved ER-resident proteins: FAM134A, FAM134B, and FAM134C (Figure 2). The proteins are encoded by three different genes and share the same LIR amino acidic sequence [20]. The FAM134C paralogue is the most expressed protein in almost all the tissues except pancreas, which mostly express FAM134B, and brain and testis, which express higher levels of FAM134A [31-32].

FAM134B is enriched in the ER sheets, whereas FAM134A and FAM134C have broader distribution within ER subdomains. FAM134B was the first mammalian ER-phagy receptor identified [20], it works at both basal and stress conditions. FAM134B has a role in the context of oesophageal and colorectal cancers [33-34] and in the pathogenesis of sensory and automatic neuropathy (HSANII) [34]. Recently has been reported the involvement of FAM134A and FAM134C in ER-phagy process [19]. All three FAM134 proteins carry a short N-terminal region and the RHD, which is composed of two hydrophobic domains flanking a hydrophilic loop, while the length of the C-terminus differs between paralogues. The RHD domain of FAM134 proteins forms wedge-shaped membrane inclusions in the ER membrane with four highly conserved structural elements: two ER anchoring transmembrane helical hairpins (TM1,2 and TM3,4), that anchor the RHD into the ER membrane; they are connected by a flexible cytoplasmic linker and two amphipathic helices (AHL and AHC) that interact with the cytoplasmic leaflet and flank the TM3,4 segment on both sides. The structure of RHD domain is essential to induce active membrane curvature as well as to sense high local curvature. The combination of these two functions maximizes the autophagic response of FAM134 proteins promoting the ER fragmentation during ER-phagy [36].

Notably, FAM134B exists in two splicing variants [21], the full-length is manly expressed in the brain, tibial nerve, adipose tissue, and testis; the truncated form (FAM134B-2) is

dominantly expressed in skeletal muscle, heart, kidney cortex, colon, pancreas, liver, and stomach [37]. The two isoforms differ from each other by transcription start sites, consequently *FAM134B-2*, consists of 6 exons which encode 356 amino acids, whereas *FAM134B-1* consists of 9 exons which encode 480 amino acids [21]. Starvation drastically induced, *in vivo*, FAM134B-2 especially in liver, kidneys, spleen, and white adipose tissue [37].

Transcriptional control of the ER-phagy pathway

ER-phagy pathway can be regulated by both transcriptional and post-translational modifications including, for instance, phosphorylation, ubiquitination, UFMylation, and acetylation. Here, the focus will be addressed on the transcriptional regulation of the ER-phagy process.

ER-phagy receptors are mostly upregulated upon starvation and ER-stress conditions (Table 1). For instance, CCPG1 is transcriptionally induced during ER stress through the canonical unfolded protein response (UPR). The transcription factor(s) regulating CCPG1 expression is still unknown, however, there are some evidence which suggest that the CCPG1 promoter can be bound by the transcription factor MIST1, required for granulogenesis of enzyme–secreting zymogenic cells [37] and regulated by IRE1/XBP1 branches of the UPR [39]. Notably, genetic deletion of CCPG1 resulted in ER expansion and increased levels of ER stress markers in pancreatic acinar cells, underlining its important contribution in maintaining ER homeostasis [25]. The ER-phagy receptor FAM134B-1 and FAM134B-2, are both upregulated during starvation-induced ER-phagy. FAM134B, but not its paralogues FAM134A and FAM134C, behaves as a “constitutively active” receptor, whose enhanced expression is sufficient to promote ER-fragmentation and ER-phagy [19]. During liver starvation, the liver specific CCAAT/enhancer binding protein beta (C/EBPb) transcription factor upregulates the expression of FAM134B-2, which is subsequently recruited to autophagosomes [21]. In glioblastoma cells, FAM134B and TEX264 transcription is strongly induced upon the treatment with the ER stressor loperamide, leading to the activation of the autophagy induced cell-death [40]. Furthermore, the transcriptional regulation of SEC62, is regulated by globular adiponectin treatment of cardiomyocytes undergoing chronic intermittent hypoxia [41]. Finally, the level of ATL3 increases during early stage of starvation [42].

Table 1. Stimuli inducing ER-phagy receptors transcription.

ER-phagy receptor	*Tissue*	*Inducer*
FAM134B	glioblastoma	loperamide-induced mTOR inhibition and ER stress (Zielke et al.,2021).
FAM134B-2	liver	Starvation (Kohno et al., 2019).
CCPG1	pancreas	chemical ER stress (Tian et al., 2010).
TEX264	glioblastoma	loperamide-induced mTOR inhibition and ER stress (Zielke et al., 2020).
SEC62	cardiomyocytes	chronic intermittent hypoxia (Zhang et al., 2020a).
ATL3	cultured cells	short starvation (Chen et al., 2019).

TFEB and TFE3: Master regulator of autophagy and lysosome

TFEB and TFE3 are members of the microphthalmia family (MiT family) of basic helix-loop-helix– leucine-zipper (bHLH-Zip) transcription factors [43]. MiT proteins share an identical basic region, which is required for DNA binding, and the highly similar HLH and Zip regions that are important for dimerization; however, outside of these regions they are quite different [43]. MiT transcription factors bind the palindromic CACGTG E-box on the DNA both as homodimers and/or heterodimers [43-44], such as other bHLH-Zip transcription factors (MYC, MAX and MAD proteins) [43]. Lysosomes are crucial components of the cellular degradation and recycling system, and their correct function is required to maintain proper cell homeostasis [45]. These organelles are indeed involved in several essential cellular processes, including endocytosis, autophagy, and lysosomal exocytosis [47]. Although lysosomes were originally described as static organelles devoted to terminal degradation of waste material, recent discoveries show that lysosomal biogenesis and function are transcriptionally regulated. Microarray analysis revealed that genes encoding for lysosomal proteins are co-expressed in different cell types and under different conditions [48]. The analysis of lysosomal gene promoters revealed that they share a common 10-base E-box-like palindromic sequence, the so-called coordinated lysosomal expression and regulation (CLEAR) motif. TFEB and TFE3 bind directly to CLEAR elements, promoting the expression of the entire network of genes that contains the CLEAR regulatory motif in their promoter (namely the CLEAR network) [48-49]. Accordingly, TFEB and TFE3 overexpression results in an increased number of lysosomes and higher levels of lysosomal enzymes, thus enhancing lysosomal catabolic activity [47].

Subcellular localization of both TFE3 and TFEB is controlled by their phosphorylation status on peculiar serine residues [49-53]. In resting cells, they are kept inactive in the cytosol with both serine phosphorylation [47;49]. Upon starvation they are de-phosphorylated, and they rapidly translocate to the nucleus thus inducing the transcription of target genes. The main protein kinase known to phosphorylate TFEB and TFE3 under nutrient-rich conditions is the mechanistic target of rapamycin complex 1 (mTORC1), the master controller of cellular growth [51-52]. Remarkably, mTORC1 activation occurs at the lysosomal membrane. In the presence of nutrients, a mechanism involving the v-ATPase complex promotes the activation of the small Rag (Ras-related GTP-binding) GTPases, which recruit mTORC1 to the lysosomal membrane, thus promoting its activation through the small GTPase Rheb [55]. Interestingly, active Rag GTPases also bind to TFEB and recruit it to the lysosomal membrane [56], thereby promoting its phosphorylation by mTORC1. Upon starvation, mTORC1 is released from the lysosomal membrane and becomes inactive. Interestingly, nutrient deprivation furthermore induces the release of lysosomal Ca2+ through the Ca2+ channel mucolipin 1 (MCOLN1), thus activating the phosphatase calcineurin, which in turn dephosphorylates TFEB and TFE3 promoting their nuclear translocation [52-54] (Figure 3). Thus, a lysosome-to-nucleus signalling pathway regulates cellular energy metabolism through TFEB and TFE3.

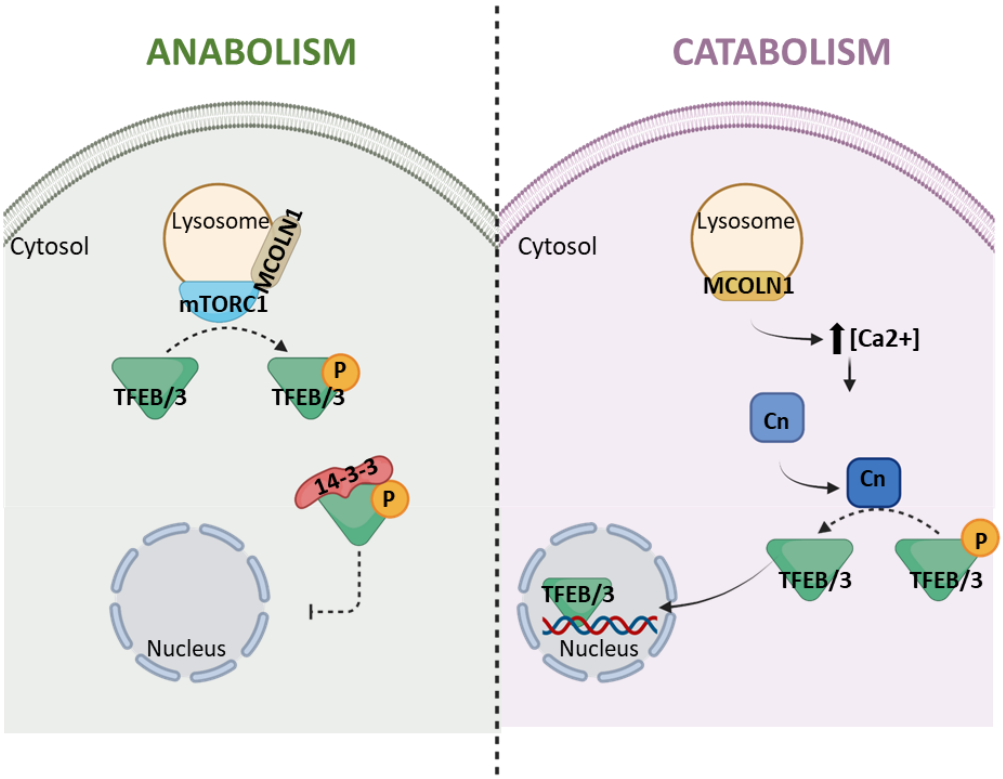

Figure 3 The lysosome to nucleus signalling pathway of TFEB Under normal feeding conditions, TFEB is phosphorylated by mTORC1 on the lysosomal surface and is sequestered in the cytoplasm by 14-3-3 proteins. During starvation mTORC1 is inactivated and Ca2+ is released from the lysosome through MCOLN1. This leads to local calcineurin

activation and TFEB dephosphorylation. Dephosphorylated TFEB is no longer able to bind 14-3-3 proteins and can freely translocate to the nucleus where it transcriptionally activates the lysosomal/autophagic pathway.

Fibroblast growth factor signalling in the growth plate

Fibroblast growth factors (FGFs) are a family of 22 polypeptides that have important roles in cell growth, differentiation, survival, and many developmental processes. The FGF members can activate one of the four tyrosine kinases FGF receptor (FGFR-1, -2, -3,-4) [57]. Several human skeletal dysplasias are caused by mutations in FGF/FGFR family members suggesting that FGF signalling is fundamental to sustain skeletal growth and development [58].

Skeletal development is highly regulated by a hierarchy of genetic, endocrine, and mechanical regulatory programs [59]. In mammals the formation of long bones is achieved by endochondral ossification, in which a cartilage template is converted into the bone. Cartilage is formed by condensation of mesenchymal cells, which subsequently differentiate into growth plate chondrocytes localized at the ends of the growing bone. Growth plate chondrocytes are arranged in columns that sequentially develop through proliferative, prehypertrophic, and hypertrophic stages. Distal hypertrophic chondrocytes undergo apoptosis and are replaced by trabecular bone and bone marrow. In a separate process, cortical bone is generated by osteoblasts derived from osteoprogenitor cells in the perichondrium [60]. Notably, in this context an essential role is played by FGFs/FGFR.

In the earliest stages of endochondral bone development, FGF receptor-2 (FGFR2) is expressed in condensing mesenchyme. As the growth plate forms, proliferating and pre-hypertrophic chondrocytes express FGFR3, while hypertrophic chondrocytes express FGFR1. Later, osteoprogenitor cells express FGFR2. Those receptors show completely different roles in bone development; among them the FGFR3 is the best understood. Remarkably, in mice the knockout of the *Fgfr3* leads to an increased rate of chondrocytes proliferation and an expansion of the length of chondrocyte columns, thus leading to long bones overgrowth [61]. Conversely, gain of function mutations in *Fgfr3* decrease chondrocytes proliferation rates and lead to shortened, disorganized columns in transgenic mice [62]. FGF receptors are mostly activated by FGF ligands. In mice, the FGF18 ligand is the most expressed by the perichondrium which surrounds the growth plate. FGF18 activates the four FGF receptors as a paracrine factor, exerting completely different functions [58-60]. It mainly regulates chondrocytes property: proliferation, differentiation and extracellular matrix deposition. Through the activation of FGFR3, it limits chondrocytes proliferation and promotes differentiation from proliferative to pre-hypertrophic chondrocyte state. Moreover, FGF18 boosts the secretion of type II collagen from proliferative chondrocytes and type X collagen from hypertrophic chondrocytes,

promoting extracellular matrix deposition. Finally, it also regulates the function of osteoprogenitor cells through the activation of FGFR2. Notably, *Fgf18* knockout mice showed severe skeletal phenotype causing by defects both in the cartilage and in the bone [58-60].

In 2015, we demonstrated that FGF18 ligand activate FGFR3 and FGFR4 in growth plate chondrocytes inducing the activation of the autophagy complex [63]. The induction of autophagy in chondrocytes is fundamental to maintain cell and tissue homeostasis clearing the endoplasmic reticulum (ER) from misfolded and aggregated type II collagen [4]. Notably, mice lacking autophagy or model of lysosomal storage diseases showed ER enlargement and retention of collagen in the ER, leading to severe skeletal defects [63-64]. Hence, the activation of autophagy at level of the ER controls chondrocytes cellular fitness.

These observations led us to hypothesize that ER-phagy in chondrocytes could be regulated by the FGF signalling. In this work, we characterized the signalling cascade activated by FGF in chondrocytes and demonstrated that FGF induces lysosome biogenesis and ER-phagy through the activation of TFEB and TFE3 transcription factors. Mechanistically, we found that TFEB and TFE3 induce the expression of the ER-phagy receptor FAM134B, hence stimulating the delivery of ER fragments into newly formed lysosomes. In addition, this process appears to be physiologically relevant during skeletal development in mice.

Results

FGF signalling induces lysosome biogenesis and ER-phagy in chondrocytes

High-resolution mass spectrometry-based proteomic analysis in Rat Swam chondrosarcoma cells (RCS) showed that FGF18 stimulation significantly downregulated ER and ribosome categories and upregulated lysosome categories compared with cells stimulated with vehicle (DMEM 5% ABS) (Figure 4A). Moreover, the prolonged (16h) FGF18 stimulation (Figure 4B,D), but not short term (4 h) (Figure 4C,E), increased lysosome numbers, as assessed by LysoTracker fluorescence intensity and by the quantification of Lysosomal Associated Membrane Protein 1 (LAMP1) positive vesicles, in RCS cells.

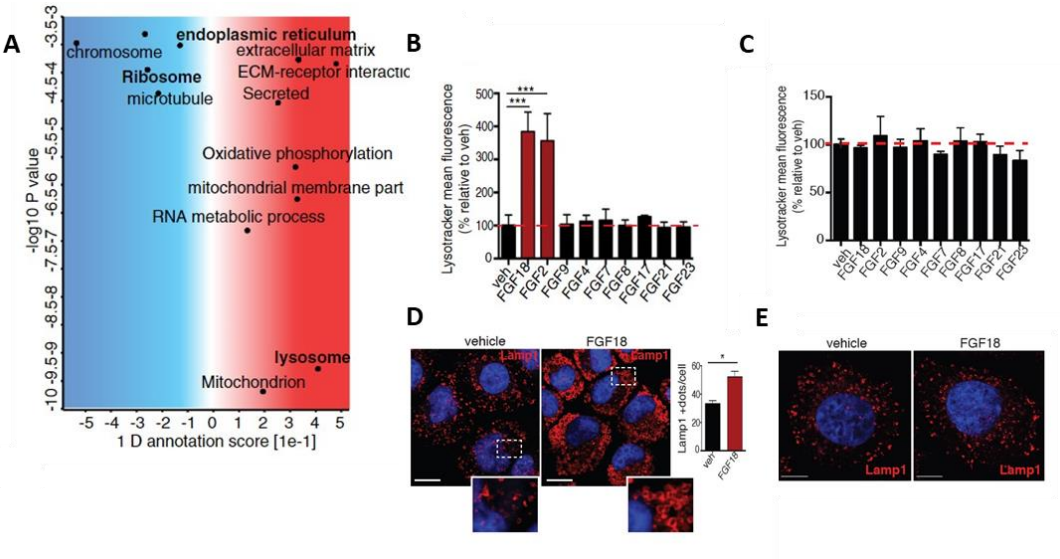

Figure 4. FGF18 induces lysosome biogenesis in chondrocytes A) MS proteomic analysis of RCS chondrocytes treated with vehicle (5% ABS) and FGF18 (50ng/ml) for 16h. Biological processes and cellular components regulated by FGF signalling are shown. FDR<0.05. N=4 biological replicates/treatment were analysed. P-value was calculated using 1D annotation enrichment test based on Wilcoxon–Mann–Whitney test. **B,C)** FACS analysis of LysoTracker dye fluorescence in RCS treated with the indicated FGF ligands (50ng/ml) for 16h (B) and for 4h (C). Fluorescence intensities were expressed as % relative to vehicle (5% ABS). Mean standard error of the mean (SEM) of N=3 biological replicates/treatment. One-way analysis of variance (ANOVA) P<0.002 (B) and P=0.005 (C); Tukey's post hoc test ***P<0.0005. **D,E)** Lamp1 immunofluorescence (red) in RCS chondrocytes treated with vehicle (5% ABS) and FGF18 (50ng/ml) for 16h (D) and for 4h (E). Nuclei were stained with DAPI (blue). Insets show magnification of the boxed area. Scale bar 15 and 2 µm (higher magnification boxes). Bar graph shows quantification of Lamp1-positive vesicles/cell. Mean standard error of the mean (SEM) of N=3 biological replicates/treatment. n=45 cells were analysed. Student's paired t-test *P<0.05.

Moreover, FGF18 prolonged-stimulation (16h) (Figure 5A), but not short term (4 h) (Figure 5B), induced the degradation of the artificial substrate DQ-BSA. Collectively these data suggested that FGF18 treatment enhances lysosome biogenesis and catabolic activity.

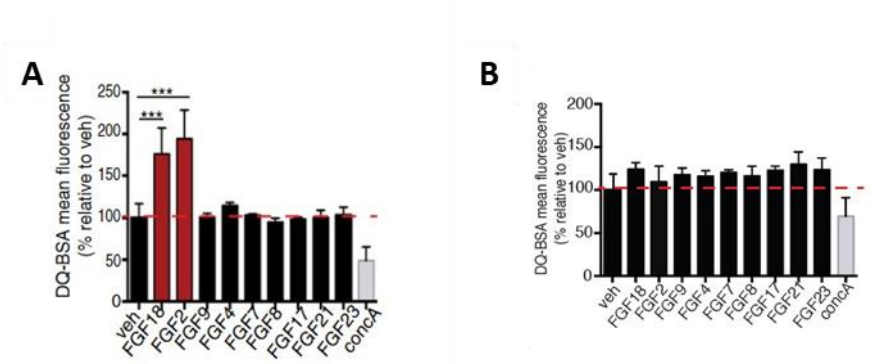

Figure 5. FGF18 promotes lysosome catabolic activity in chondrocytes A,B) FACS analysis of DQ-BSA dye fluorescence in RCS treated with the indicated FGF ligands (50ng/ml) for 16h (A) and for 4h (B). Concanamycin A (100 nM;1h) was used as negative control to inhibit lysosomal degradation. Fluorescence intensities were expressed as % relative to vehicle (5% ABS). Mean standard error of the mean (SEM) of N=3 biological replicates/treatment. One-way analysis of variance (ANOVA)P<0.002 (B) and P=0.005 (C); Tukey's post hoc test ***P<0.0005.

Notably, we observed, by transmission electron microscopy (TEM), that long term FGF18 stimulation and inhibition of lysosome degradation, by Bafilomycin A1 (inhibitor of vacuolar H^+-ATPase) treatment, led to the accumulation of ER membranes into the lysosome. Notably, but not other membranes, such as from mitochondria, were detected (Figure 6A). Those results suggested that FGF18 promotes ER degradation and lysosome biogenesis in RCS cell line. To corroborate these results, we took advantage from the use of an ER-phagy Tandem Report assay (EATR) [23]. RAMP4 protein is fused to eGFP-mCherry construct to follow lysosomal degradation of ER membranes. Cytosolic ER (pH∼7) should maintain both GFP and mCherry fluorescence, whereas GFP fluorescence should be quenched when ER membranes where targeted to acidic lysosomal vesicles (pH<4), showing mCherry fluorescence alone (Figure 6B). RCS treated with FGF18 showed acidified ER compared to control cells, instead FGF18 failed to induce lysosomal degradation of the ER in autophagy deficient cells (ATG9 KO, ATG7 KO and Beclin-1 KO) (Figure 6C). Taken together, these data demonstrated that FGF induced lysosome biogenesis and ER-phagy in chondrocytes.

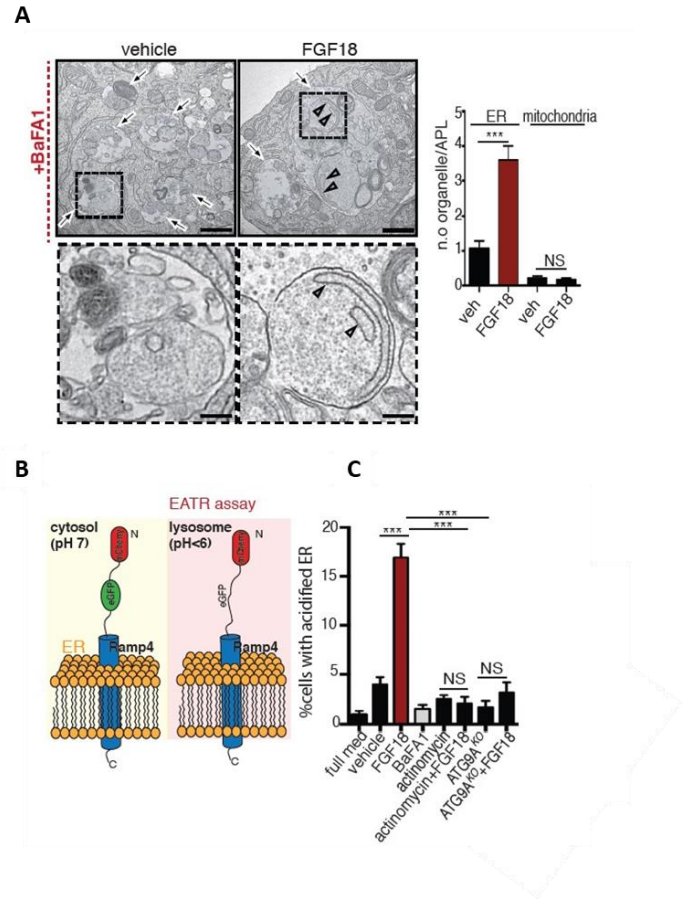

Figure 6. FGF18 regulates ER-phagy in chondrocytes A) Representative TEM images of RCS chondrocytes treated with 5% ABS (vehicle) and FGF18 (50 ng/ml) for 16 h. BafA1 (100 nM; 4 h) was used to inhibit lysosome activity. Arrows indicate lysosomes. Higher magnification insets showed the presence of ER membranes decorated with ribosomes (arrowheads). Scale bar 500 nm. Quantification shows average number of ER membranes and mitochondria number/lysosome vesicle (Lys). Mean ± standard error of the mean (SEM) of N = 3 biological replicates/treatment. ER fragment/vesicle n=60 (vehicle) and n=72 (FGF18) cells were analysed; mitochondria number/vesicle: n=40 (vehicle) and n=72 (FGF18) cells were analysed. Student's paired t-test ***P < 0.0005; NS, not significant. **B)** Schematic representation of EATR assay: eGFP fluorescence, but not mCherry, is lost at acidic pH. **C)** Chondrocytes with indicated genotypes (ctrl=wild type) were treated with FGF18 (50 ng/ml; 16h) and BafA1 (200 nM; 3h) where indicated. ER acidification was measured by FACS. Mean ± standard error of the mean (SEM) of N = 3 biological replicates. One-way analysis of variance (ANOVA) P < 0.0001; Tukey's post hoc test ***P < 0.0005; **P < 0.005; NS, not significant.

FGF18 inhibits the PI3K signalling cascade through FGFR3/4 receptors

FGF ligands can bind to four receptor tyrosine kinases (FGFR1-4; [58]). To test which receptor is activated by FGF18, we deleted in RCS cells each of the FGFRs, alone or in combination, using CRISPR/Cas9 approach. The FGF18-dependent induction of lysosome biogenesis and activity is abolished in RCS lacking FGFR3 (FGFR3 KO) and partially inhibited in cells lacking FGFR4 (FGFR4 KO), while it remained unmodified in cells lacking FGFR1 and/or FGFR2 receptors (Figure 7 A,B).

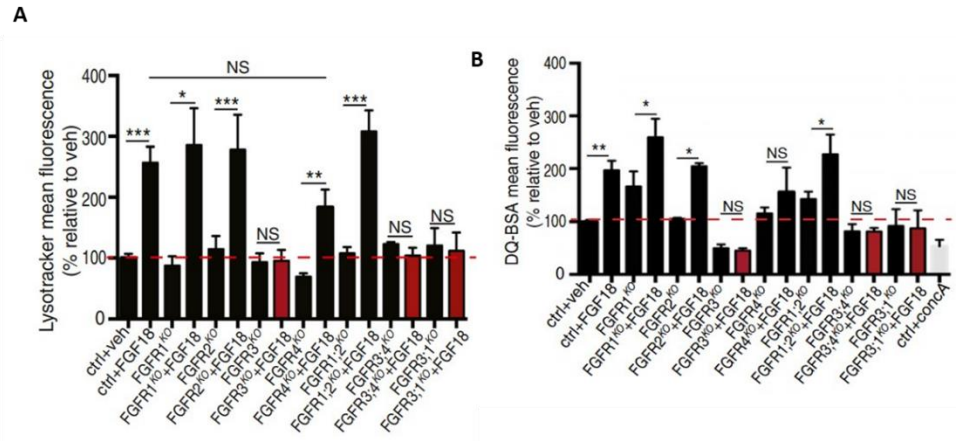

Figure 7. FGF18 induces lysosome biogenesis and activity through FGFR3 and FGFR4 A) FACS analysis of LysoTracker dye fluorescence in RCS with indicated genotypes (ctrl = wild type) treated with FGF18 (50 ng/ml for 16 h). Fluorescence intensities were calculated as % relative to vehicle (5% ABS). Mean ± standard error of the mean (SEM) of N=3 biological replicates. One-way analysis of variance (ANOVA) P = 0.024.; Tukey's post hoc test *P < 0.05; NS, not significant. **B)** FACS analysis of DQ-BSA dye fluorescence in chondrocytes with indicated genotypes (ctrl=wild type) treated with FGF18 (50ng/ml) for 16h. Concanamycin A was used at 100nM for 1h to inhibit lysosomal degradation. Fluorescence intensities were expressed as % relative to vehicle (5% ABS). Mean ± standard error of the mean (SEM) of N=3 biological replicates/treatment/genotype. Analysis of variance (ANOVA) P=0.00279; Tukey's post hoc test **P<0.005; *P<0.05; NS, not significant.

Notably, FGFR3/4 double knock-out (dKO) chondrocytes showed: i) inhibition of lysosomal enzymatic activity (β-Hexosaminidase and β-Glucuronidase) (Figure 8A,B), ii) enlarged lysosomes containing undigested membranes (Figure 8C;D) and iii) impaired ER-phagy (Figure 8E). These data suggested that FGF18 promotes ER-phagy and lysosome biogenesis through FGFR3 and FGFR4.

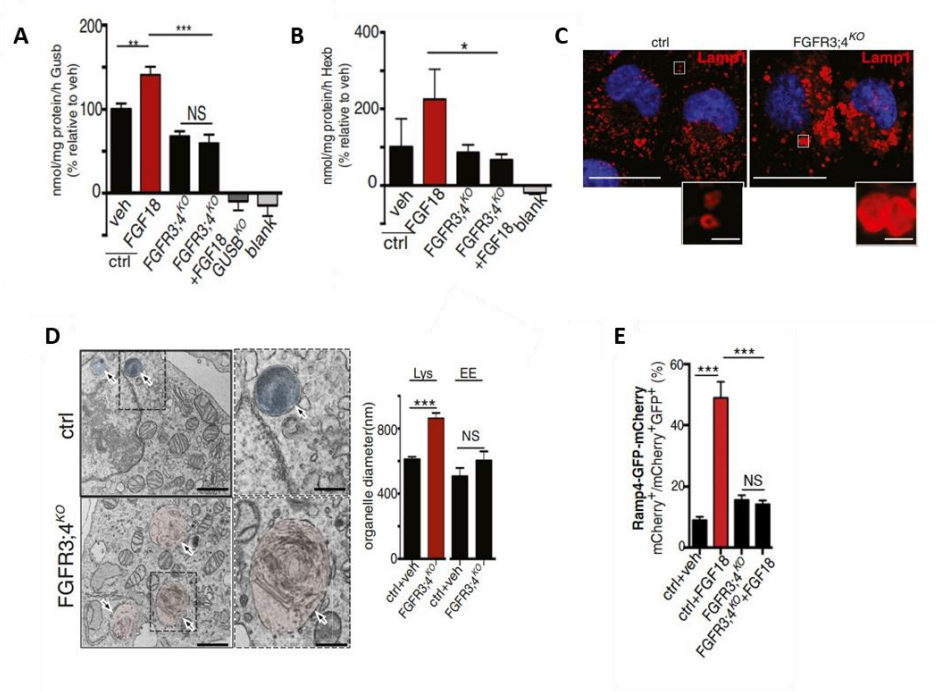

Figure 8 FGF18 induces lysosome biogenesis and ER-phagy through FGFR3 and FGFR4 A-B) Enzymatic assay of lysosomal β-glucuronidase and β-hexosaminidase enzymes in chondrocytes with indicated genotypes (ctrl=wild type) treated with FGF18 (50 ng/ml) for 16 h. Mean ± standard error of the mean (SEM) N=5 biological replicates (Gusb) and N=6 biological replicates (Hexb). One-way analysis of variance (ANOVA) $P < 0.001$; Tukey's post hoc test ***$P < 0.0005$; **$P < 0.05$; *$P < 0.05$; NS, not significant. Blank represents the value of the substrate alone. **C)** Representative immunofluorescence staining of Lamp1 (red) in chondrocytes with indicated genotypes. Higher magnification insets showed enlarged lysosomes in FGFR3/4KO chondrocytes. Nuclei were stained with DAPI (blue). Scale bar 15 and 5 µm (higher magnification boxes). Representative images of N=3 biological replicates/treatment. **D)** Representative TEM images of wild type (ctrl) and FGFR3;4KO chondrocytes showing lysosomes (arrows); scale bar 500 nm. Insets show enlargement of lysosomes; scale bar 250 nm. Quantification of organelle diameter (nm). Mean ± standard error of the mean (SEM) of N=3 biological replicates/genotype. Student's unpaired t test ***$P < 0.0005$; NS, not significant. n=45 (ctrl) and n=51 (FGFR3;4KO) cells were analysed. Lys=lysosome; EE=endosome. **E)** EATR assay. Chondrocytes with indicated genotypes (ctrl=wild type) treated with FGF18 (50ng/ml;16h) where indicated. ER acidification was measured by FACS. Mean ± standard error of the mean (SEM) of N=17 (veh), N=17 (FGF18), N=4 (FGFR3;4KO); N=4 (FGFR3;4KO FGF18) biological replicates. One-way analysis of variance (ANOVA) $P<0.0001$; Tukey's post hoc test ***$P<0.0005$; NS, not significant.

Next, we performed mass spectrometry (MS) phospho-proteomic analysis in control and FGFR3/4 dKO RCS stimulated with FGF18 to identify the downstream signalling cascade. The Insulin/PI3K/mTORC pathway was the most downregulated upon FGF18 stimulation in control RCS but was not altered in FGFR3/4 dKO RCS (Figure 9A). Western blot analysis showed that FGF18 stimulation induced downregulation of AKT (S473) and pP70S6K (T389) phosphorylation on aminoacidic residues targeted by mTORC kinases in control RCS (Figure 9B). The MAP kinase pathway is still activated by FGF18 treatment, as observed by phosphorylation of ERK kinase (Figure 9B), suggesting that FGF signalling specifically inhibits Insulin/PI3K /mTORC pathway

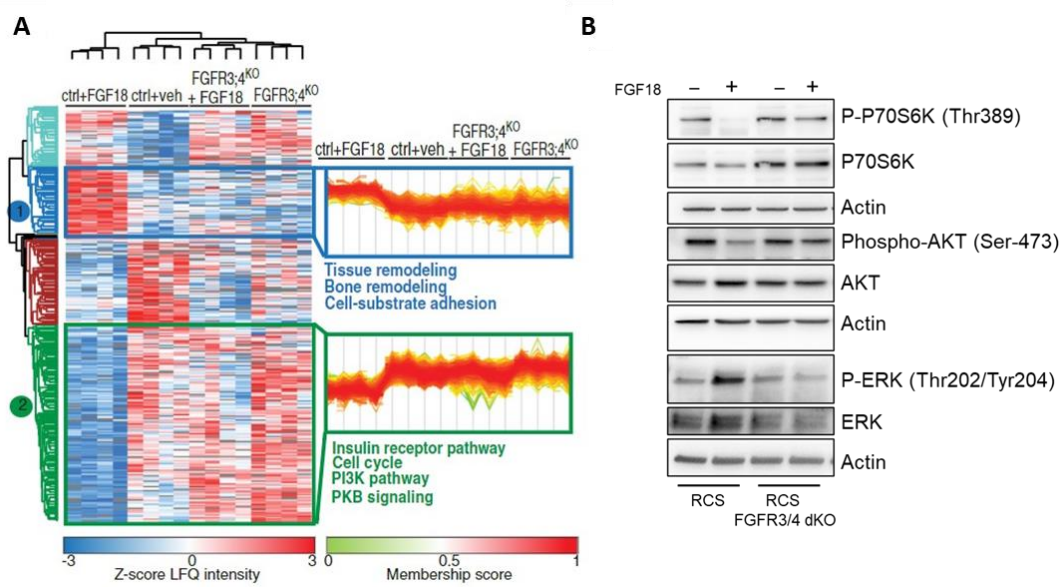

Figure 9. FGF18 inhibits the insulin/PI3K pathway A) MS phospho-proteomics analysis of RCS with indicated genotypes (ctrl=wild type) treated with vehicle (5% ABS) and FGF18 (50ng/ml) for 16h, showing biological processes regulated by FGF signalling (in blue: upregulated, in green: downregulated). N=4 biological replicates were analysed. FDR<0.05 **B)** Representative Western blot analysis of p-P70S6K (T389), P70S6K, p-AKT (T308), AKT, p-ERK (Thr202/Tyr204), and ERK in RCS chondrocytes treated with vehicle (5% ABS) and FGF18 (50 ng/ml) ON. β-actin was used as a loading control. N=3 independent experiments.

FGF18 induces lysosome biogenesis and ER-phagy transcriptionally

FGF18 enhances lysosome biogenesis, inhibits mTORC pathway, and promotes ER-phagy. Next, we investigated if FGF signalling could trigger a transcriptional regulation of lysosome and ER-phagy in RCS cells. QuantSeq 3' mRNA sequencing gene expression analysis (GSE120516) followed by GOEA, with the output restricted to cellular compartment terms (CC_FAT), and KEGG pathway analysis revealed that upon FGF-treatment, lysosome is the most upregulated category (Figure 10A). FGF stimulation failed to induce LysoTracker fluorescence (Figure 10B), and ER-phagy (Figure 10C) in chondrocytes treated with the transcription inhibitor Actinomycin, suggesting that FGF-

signaling promoted lysosome biogenesis and ER-phagy in chondrocytes via a transcription dependent pathway.

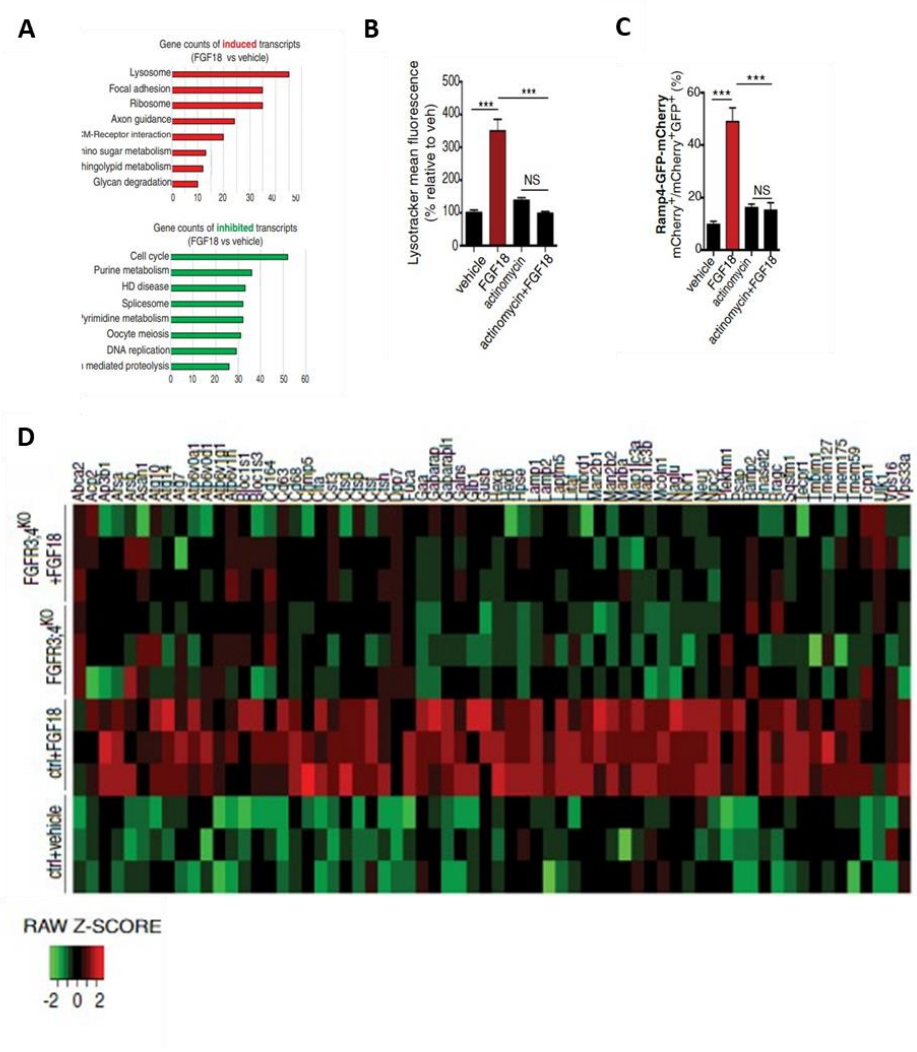

Figure 10. FGF18 induces lysosome biogenesis and ER-phagy via a transcriptional control mechanism A) KEGG pathway analysis of Quantsec gene expression analysis in RCS chondrocytes treated with vehicle (5% ABS) and FGF18 (50 ng/ml) for 16h, showing upregulated (red) and downregulated (green) biological processes and cellular components. **B)** FACS analysis of LysoTracker dye fluorescence in RCS chondrocytes treated with FGF18 (50ng/ml) for 16h. Actinomycin (1µg/ml) was added for the last 4h. Fluorescence intensities were calculated as % relative to vehicle (5% ABS). Mean ± standard error of the mean (SEM) of N=3 biological replicates. One-way analysis of variance (ANOVA)P=0.0002; Tukey's post hoc test ***P<0.0005; NS, not significant. **C)** EATR assay. Chondrocytes were treated with FGF18 (50ng/ml; 16h) and actinomycin (1µg/ml; last 4h) where indicated. ER acidification was measured by FACS. Mean standard error of the mean (SEM) of N=17 (veh), N=17 (FGF18), N=5 (actinomycin), and N=5 (actinomycin+FGF18) biological replicates. One-way analysis of variance (ANOVA) P<0.0001; Tukey's post hoc test ***P<0.0005; NS, not significant. **D)** Heatmap of lysosomal and autophagy gene expression in RCS chondrocytes with indicated genotypes (ctrl=wild type), treated with vehicle (5% ABS) and FGF18 (50ng/ml) for 16h. FDR<0.05. N=3 biological replicates/treatment were analysed. In green: downregulated; in red: upregulated gene expression.

In addition, the QuantSeq analysis revealed that FGF18 significantly induced 66 lysosomal and autophagy genes in WT but not in FGFR3/4 dKO RCS (Figure 10 D). By qRT-PCR analysis we also evaluated the expression level of different ER-phagy receptors, and among them, FGF18 stimulation strongly and significantly increased mRNA and protein levels of the *Fam134b* gene (Figure 11A-B). qRT-PCR was performed using primers that anneal to a DNA region shared by all the *Fam134b* isoforms. Notably, FGF18 stimulation had moderate or null effects on the expression of other members of the FAM134 family (*Fam134a* and *Fam134c*) and on other ER-phagy receptors (*Ccpg1*, *Atl3*, *Sec62*, *Tex264*, *Rtn3L*, *Atl1*, *Calcoco1* and *Sqstm1*) (Figure 11A).

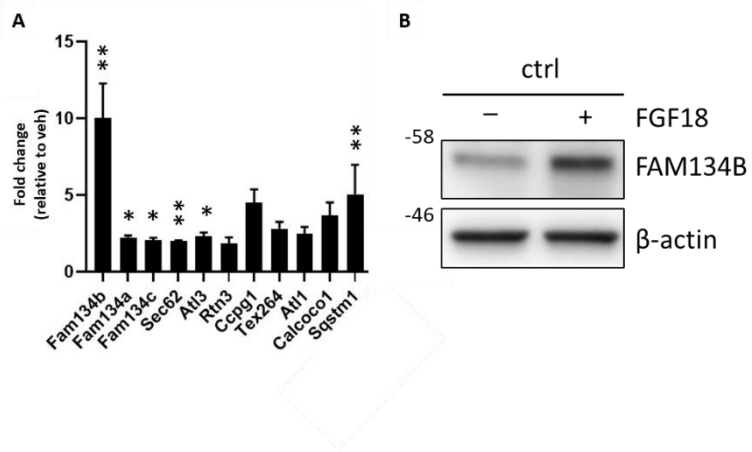

Figure 11. FGF18 enhances *Fam134b* expression A) qRT–PCR analysis of ER-phagy receptors in RCS chondrocytes. Gene expression was analysed after FGF18 (50ng/ml) treatment for 16h. Fold change values were relative to vehicle (5% ABS) and normalized to *Cyclophilin* gene. Mean ± standard error of the mean (SEM) of N=3 biological replicates/treatment. Student's paired-test **P<0.005; *P<0.05. **B)** Representative Western blot analysis of FAM134B in RCS chondrocytes treated with vehicle (5% ABS) and FGF18 (50 ng/ml) ON. β-actin was used as a loading control. N=3 independent experiments.

Moreover, we found that ER-phagy is also functionally inhibited upon FGF18 stimulation in RCS which brings the deletion of the C terminal region of FAM134B (which contains the LIR domain for incorporation of ER membranes into the AVs) (Fam134bΔLIR) (Figure 12A-B). Thus, suggested that FGF18 induces ER-phagy via FAM134B. Overall, these data suggested that FGF18 transcriptionally regulates lysosomal biogenesis and ER-phagy.

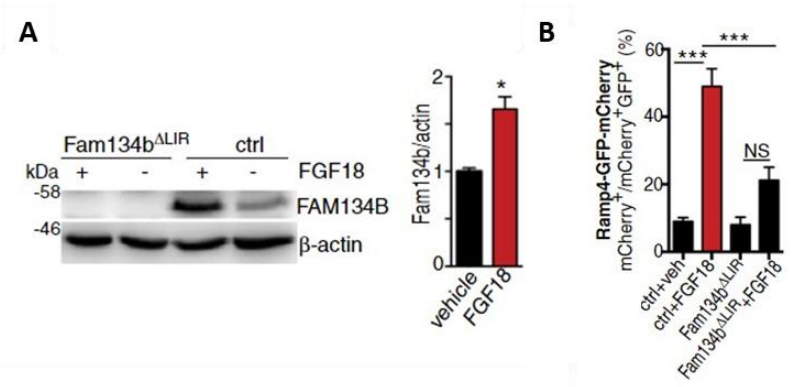

Figure 12. FGF18 induces ER-phagy via FAM134B A) Western blot analysis of FAM134B in chondrocytes with indicated genotypes (ctrl=wild type) treated with FGF18 (50ng/ml) for 16h. Representative images of N=3 biological replicates/treatment. b-actin was used as a loading control. Bar graph showed quantification of FAM134B band intensity normalized to b-actin. Mean ± standard error of the mean (SEM). Student's paired t-test, *P<0.05. **B)** EATR assay in RCS with indicated genotypes (ctrl=wild type) showing % of cells with acidified ER by FACS analysis. FGF18 was used at 50ng/ml for 16h. Mean ± standard error of the mean (SEM) of N=4 biological replicates/treatment/genotype. One-way analysis of variance (ANOVA)P<0.0001; Tukey's post hoc test ***P<0.0005; NS, not significant.

FGF signalling activates ER-phagy via TFEB/TFE3-mediated FAM134B induction

We postulated that FGF18 could activate MiT/TFE transcription factors, such as TFEB and TFE3, that in turn could control the transcription of lysosomal and autophagy genes. We analysed the promoter of genes regulated by FGF18 and we observed that most of them contain one or more CLEAR site, a ten bases E-box palindromic sequence that could be recognized by the MiT/TFE transcription factors. Furthermore, the kinases mTORC1 and AKT (downregulated by FGF18 as shown in Figure 9) phosphorylate and inhibit TFEB and TFE3, which in turn transcriptionally up-regulate lysosome biogenesis and autophagy (see Introduction).

In line with this hypothesis, FGF18 induced TFEB and TFE3 nuclear translocation in control but not in cells lacking FGFR3/4 (Figure 13A). Notably, FGF18 promoted TFEB transcriptional activation, as demonstrated by the increased binding to the promoter of the target gene Mucolipin-1 (Figure 13B). Moreover, by qRT-PCR we observed that FGF18 stimulation induced lysosomal genes expression and this induction was impaired in chondrocytes lacking both TFEB and TFE3 (Figure 13C). The overexpression of a constitutively active form of TFEB (S142A:S211A) and TFE3 (S246A:S312A) rescued lysosomal gene expression in FGFR3/4KO cells (Figure 13D). Collectively, these data suggested that FGF signaling induced TFEB and TFE3 nuclear translocation and activation.

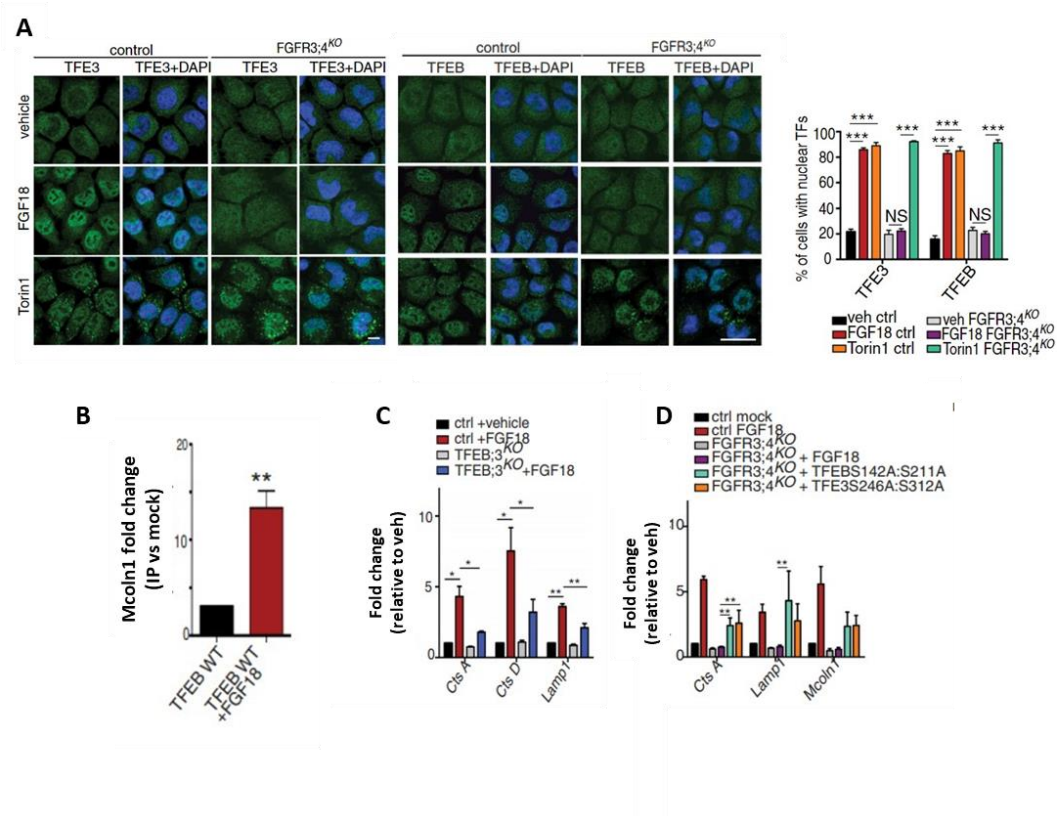

Figure 13. FGF18 activates TFEB and TFE3 transcription factors A) TFE3 (left, green) and TFEB (right, green) subcellular localization in RCS with indicated genotypes (control=wild type) treated with FGF18 (50ng/ml) for 16h. Torin1 (1µM for 2h) was used as positive control. Nuclei were stained with DAPI (blue). Bar graph shows quantification (expressed as%) of cells with nuclear TFE3 and TFEB. Mean ± standard error of the mean (SEM) of N=3 biological replicates; n=80 (TFE3) and n=70 (TFEB) cells/experiment were analysed. One-way analysis of variance (ANOVA) $P=3.23e^{-12}$ (TFEB), $P=2.48e^{-11}$ (TFE3); Tukey's post hoc test ***P<0.0005; NS, not significant. **B)** Chromatin immunoprecipitation experiment in TFEB-WT overexpressing cells treated with FGF18 (50 ng/ml) for 16 h, showing enrichment of TFEB binding on Mucolipin-1 promoter upon FGF18 treatment. N=3 biological replicates. Mean ± standard error (sd). Student's unpaired t-test **P < 0.005. **C)** qRT–PCR analysis of lysosomal genes in wild type (ctrl) and TFEB;3KO RCS treated with FGF18 (50 ng/ml for 16 h). Fold change values were relative to vehicle and normalized to Cyclophilin gene. Mean ± standard error of the mean (SEM) of N=4 biological replicates. Analysis of variance (ANOVA) CTSA P=0.0003; CTSD P=0.0065; Lamp1 P=0.00002; Tukey's post hoc test **P < 0.005; *P < 0.05. **D)** qRT–PCR analysis of lysosome genes expression in chondrocytes with indicated genotypes (ctrl=wild type). TFEB-S142A:S211A and TFE3-S246A:S312A mutant plasmids were overexpressed for 48 h; FGF18 (50 ng/ml) treatment was for 16 h. Values were normalized to Cyclophilin gene and expressed as fold change relative to cells transfected with empty vector (mock). Mean ± standard error of the mean (SEM) of N = 3 biological replicates. One-way analysis of variance (ANOVA) Tukey's post hoc test **P < 0.005.

We tested whether TFEB and TFE3 also regulate ER-phagy in chondrocytes. The increase in *Fam134b* by FGF18 stimulation was blunted, at both mRNA and protein levels, in TFEB/3 dKO RCS (Figure 14A, B). FGF18 treatment induced the accumulation of CLIMP63, that is an ER resident protein, inside lysosomes of RCS treated with BaFA1 but not in cells that lack TFEB/TFE3 (Figure 14C). Notably, by LC3-RFP-GFP tandem assay, we found that FGF18 was still able to induce the autophagy flux in TFEB/3KO cells (Figure 14D), suggesting that, at least in our model, FGF18 could regulate basal autophagy also with other TFEB-independent mechanisms. Conversely, our data suggested that FGF-dependent activation of TFEB/TFE3 is essential for ER-phagy.

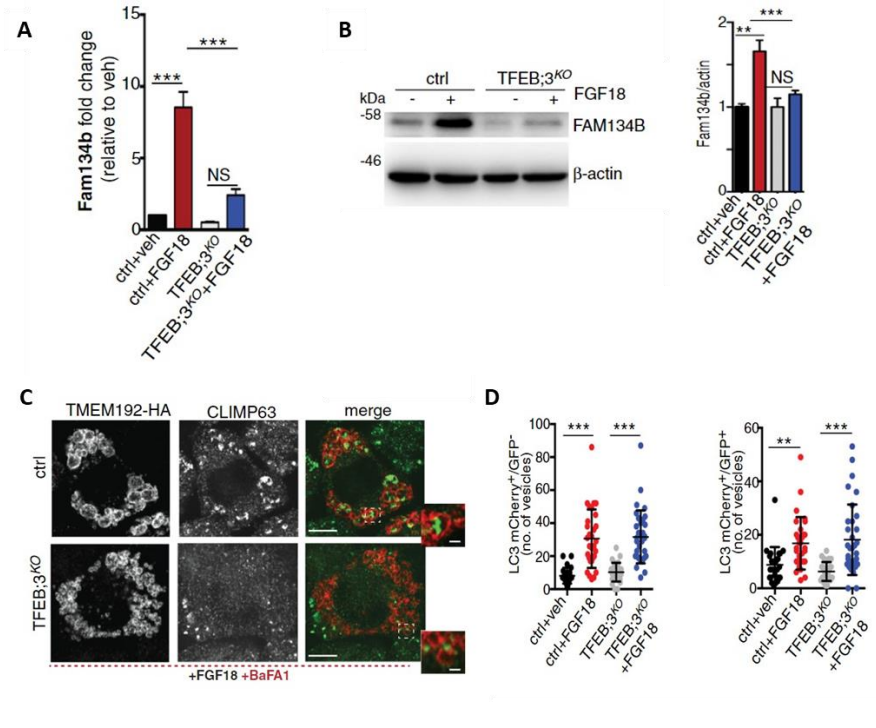

Figure 14. FGF signalling regulates *Fam134b* transcriptional levels through TFEB and TFE3 A) qRT–PCR analysis of *Fam134b* gene expression in chondrocytes with indicated genotypes (ctrl=wild type) treated with vehicle (5% ABS) or with FGF18 (50ng/ml; 16h). Fold change values were relative to vehicle and normalized to Cyclophilin gene. Mean ± standard error of the mean (SEM) of N=3 biological replicates. One-way analysis of variance (ANOVA) P<0.0001: Tukey's post hoc test ***P<0.0005; NS, not significant. B) Western blot analysis of FAM134B protein in chondrocytes with indicated genotypes treated with vehicle (5% ABS) and FGF18 (50ng/ml) for 16h. β-actin was used as a loading control. Representative image of N=3 biological replicates. Bar graph showed quantification of FAM134B normalized to β-actin. One-way analysis of variance (ANOVA) P<0.0001; Sidak's multiple comparison test ***P<0.0005; **P<0.005; NS, not significant. **C)** Immunofluorescence of CLIMP63 (green) and TMEM192-HA (lysosomes, red) in control and TFEB;3 KO RCS treated with FGF18 (50ng/ml for16h). BaFA1 was used at 100nM for 3h. Scale bar15 and 2µm (higher magnification boxes). **D)** Data plots show quantification of mCherry+vesicles/cell (autolysosomes) and mCherry+/GFP+vesicles/cell (autophagosomes) in wild type (ctrl) and TFEB;3KO cells treated with vehicle (veh) or FGF18. N=3 independent experiments. Mean ± standard error of the mean (SEM) of N=24 (wild type treated with 5% ABS, veh), N=30 (wild type treated with FGF18), N=27 (TFEB;3KO veh), N=33 (TFEB;3KO FGF18) cells. Student's unpaired t-test ***P<0.0005; **P<0.005.

Furthermore, the overexpression of TFEB, TFE3, and MITF, but not of FOXO3 or RUNX2, significantly increased mRNA of *Fam134b* in chondrocytes with a synergistic effect upon FGF18 stimulation (Figure 15A). Chromatin immunoprecipitation (ChIP) and luciferase assay experiments demonstrated that TFEB binds to a CLEAR site that is in the third intron of the *Fam134b* gene, in correspondence of the alternative transcript start site of the *Fam134b* isoform 2 (Figure 15 B, C). Consistently, FGF18 treatment predominantly upregulated the *Fam134b-2* isoform in RCS, largely in a TFEB/TFE3-dependent manner, as demonstrated by qRT-PCR analysis (Figure 15D). These data indicate that *Fam134b* is a newly identified target gene of MiTF/TFE factors.

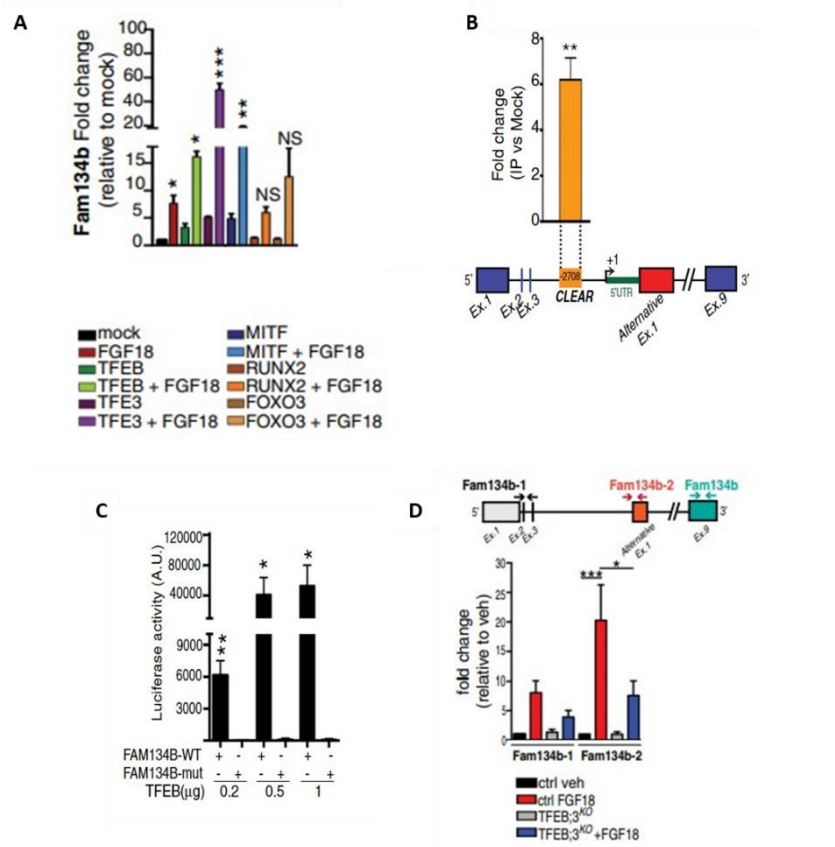

Figure 15. FGF18 induces *Fam134b-2* via TFEB activation in RCS A) qRT–PCR analysis of Fam134b gene expression in RCS transfected with indicated transcription factors for 48 h. FGF18 (50 ng/ml; 16 h) was added where indicated. Values were normalized to *Cyclophilin* gene and expressed as fold change relative to mock-transfected cells. Mean ± standard error of the mean (SEM) of N=4 biological replicates/treatment. Student's paired t-test *P < 0.05 and one-way analysis of variance (ANOVA) P = 0.0001; Tukey's post hoc test ***P < 0.0005; **P < 0.005; NS, not significant. **B)** ChIP analysis of TFEB binding to *Fam134b* DNA in RCS cells transfected with TFEB-3XFLAG. Numbers in the CLEAR site (yellow box) refer to the distance [in base pairs] from the transcriptional start site (+1) of *Fam134b-2* gene. Immunoprecipitated DNA was normalized to the input and plotted as relative enrichment over the mock control. Bar graph shows fold change enrichment; mean ± standard error of the mean (SEM) of N=3 independent experiments. Student's unpaired

t-test**P<0.005. **C)** Luciferase assays in RCS chondrocytes using as promoter a 0.7kb genomic *Fam134b* DNA fragment containing a wild type (FAM134B-WT) or a deleted (FAM134B-mut) version of the CLEAR site. TFEB plasmid transfection amount and FGF18(50ng/ml for16h) treatments are indicated. Mean ± standard error of the mean (SEM) of N=3 biological replicates. Student's paired t-test *P<0.05; **P<0.005. **D)** Schematic representation of *Fam134b* DNA locus. Arrows indicate the positions qPCR primer pairs used to detect *Fam134b-1* (black arrows), *Fam134b-2* (brown arrows), or both (turquoise arrows) isoforms. qRT–PCR of *Fam134b-1* and *Fam134b-2* isoforms in RCS with indicated genotypes (veh and FGF18 refer to treated wild-type chondrocytes). FGF18 (50 ng/ml; 16h) was added where indicated. Values were normalized to *Cyclophilin* gene and expressed as relative to mock transfected cells. Mean standard error of the mean (SEM) of N=4 (*Fam134b-1*) and N=5 (*Fam134b-2*) biological replicates/treatment. One-way analysis of variance (ANOVA) P=0.0013; Sidak's multiple comparison test ***P<0.0005; *P<0.05.

The overexpression of both Fam134b-1 and, most importantly, Fam134b-2 in Fam134bΔLIR cells rescued Climp63 accumulation inside the lysosome upon FGF18 stimulation (Figure 16), thus also corroborating the functional regulation of ER-phagy by Fam134b isoform 2.

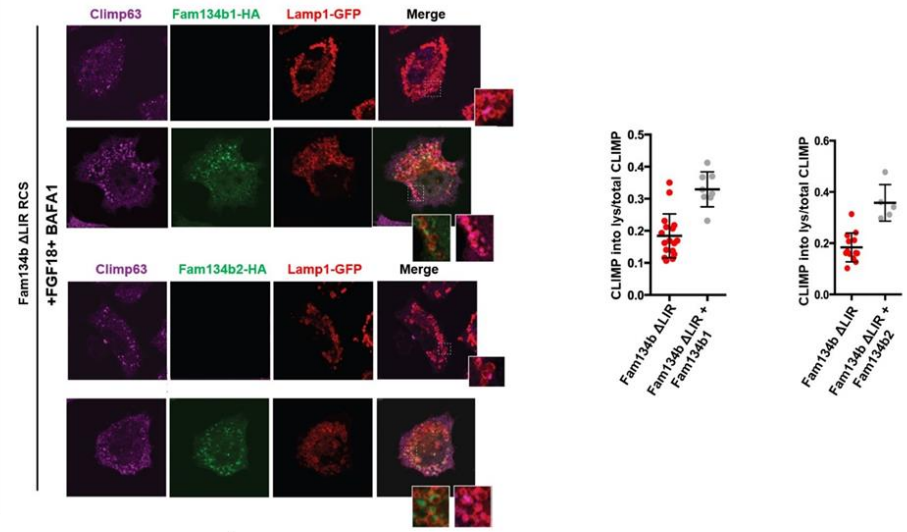

Figure 16. Fam134b-1 and Fam134b-2 rescued CLIMP63 lysosomal accumulation in Fam134bΔLIR cells Immunofluorescence staining of CLIMP63 (violet) and lysosomes (GFP-Lamp1, red) in FAM134bΔLIR RCS chondrocytes transfected with Fam134b-1 and Fam134b-2 HA-tagged (green) plasmids upon FGF18 treatment (50 ng/ml for 16h). BafA1 (100nM; 4h) was used to inhibit lysosomal degradation. Insets show magnification of CLIMP63 accumulation into lysosomes. Scale bar 10 and 2 µm (higher magnification boxes).

FGF signalling induces ER-phagy in mice cartilage

Subsequently, we tested the physiological relevance of ER-phagy regulation by FGF by analysing femoral growth plates in mice lacking both FGFR3 and FGFR4 (FGFR3/4 dKO). FGFR3/4 dKO mice were growth-retarded compared with control (Figure 17A) and histological examination of the femoral growth plate revealed an altered organization of

hypertrophic chondrocytes in FGFR3/4KO mice (Figure 17B). In addition, FGFR3/4 dKO growth plates showed down-regulation of *Fam134b-2* at mRNA level (Figure 17C) and ER cisterna enlargement (Figure 17D). Collectively, these observations strongly suggest that FGF signalling is a physiological regulator of FAM134B-mediated ER-phagy in chondrocytes during endochondral ossification.

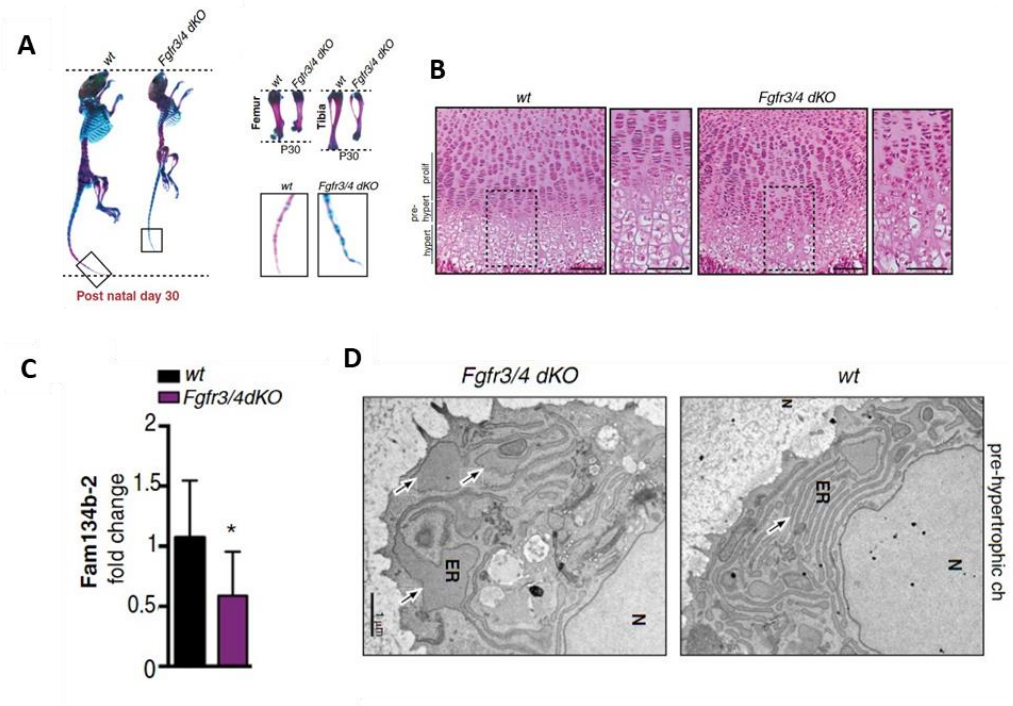

Figure 17. FGF signaling controls ER-phagy *in vivo* A) Representative images of Alcian Blue (cartilage) and Alizarin Red (bone) skeletal staining showing growth retardation inFgfr3/4 dKO mice compared to age/sex wild-type littermate at post-natal day 30. (Right) Femur, tibia, and tail details. **B)** Hematoxylin/eosin staining of femoral growth plate sections from wild-type and Fgfr3/4 dKOmice. Higher magnification insets showed a disorganized hypertrophic chondrocyte layer, in Fgfr3/4dKO mice. Scale bar 60 µm. **C)** qRT–PCR analysis of *Fam134b-2* expression from growth plate of mice with indicated genotypes. N=8 (wt mice) and N=9 (Fgfr3/4dKO mice) were analysed. Values were normalized to Hprt gene and expressed as fold change relative to control. Mean ± standard error of the mean (SEM). Student's unpaired t-test*P<0.05. **D)** Representative TEM images of growth plate chondrocytes from mice with indicated genotypes. Arrows indicated the ER. N=nucleus. Scale bar 1 µm.

Next, we explored the consequences of ER-phagy inhibition in chondrocytes, *in vitro*. MS-based proteomics analysis demonstrated that the downregulation of ER proteins induced by FGF18 was significantly inhibited in Fam134bΔLIR cells (Figure 18A), further demonstrating the requirement of FAM134B in FGF-mediated ER-phagy. Notably, the downregulation of ribosomal proteins upon FGF was also inhibited in Fam134bΔLIR cells, suggesting that ribosome turnover is influenced by FAM134B-mediated ER-phagy (Figure 18A). Secretome analysis using tandem mass-tag proteomics demonstrated that FGF-regulated protein secretion was impaired in Fam134bΔLIR cells (Figure 18B). We observed that the secretion of angiogenic (VEGFs, CTGF) and matrix remodeling (Mmp13) factors,

well known marker of bone differentiation, was impaired in Fam134bΔLIR cells (Figure 18B).

Overall, these data suggested that FAM134B-mediated ER-phagy may play an important role in chondrocytes differentiation during skeletal development.

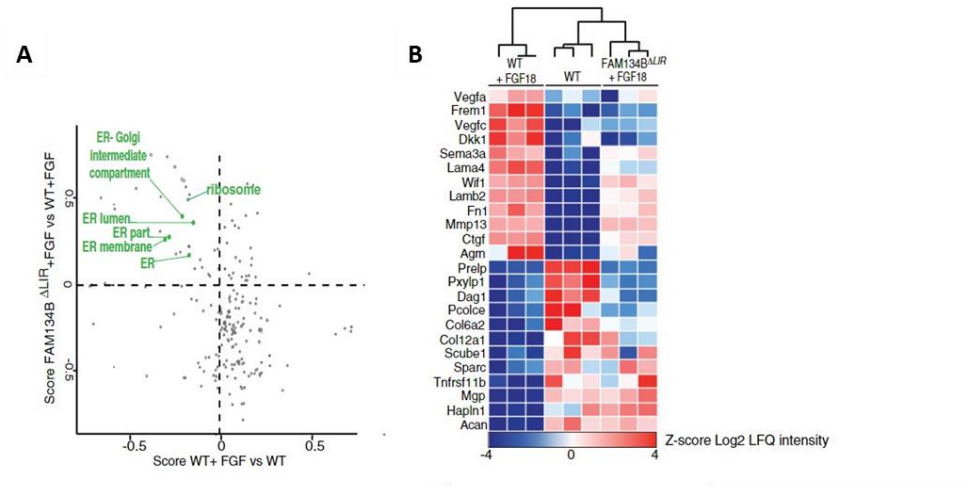

Figure 18. FAM134B is required for protein secretion in RCS (A) Scatter plot of cellular compartments and biological processes regulated by FGF18 in a FAM134B-dependent manner. Student's t-test difference between wild-type and Fam134bΔLIR cells. N=3 biological replicates/treatment/genotype were analysed. FDR<0.05. **(B)** Tandem mass tag secretome analysis of chondrocytes with indicated genotypes and treatments. FAM134B-dependent secreted proteins are shown; N=3 biological replicates/treatment/genotype were analysed.

Discussion

In this work we demonstrated that the autophagy of the ER (ER-phagy) responds to developmental and extracellular cues in chondrocytes, such as FGF signalling. Particularly, we defined the signalling pathway downstream the activation of the FGFR3 and FGFR4 receptors upon FGF18 stimulation, which in turn activates TFEB and TFE3 transcription factors, leading to the induction of *FAM134B* expression, well known ER-phagy receptor [20] (Figure 19). The activation of ER-phagy in chondrocytes may provide a possible model by which FGF signalling may regulate chondrocyte functions during endochondral ossification.

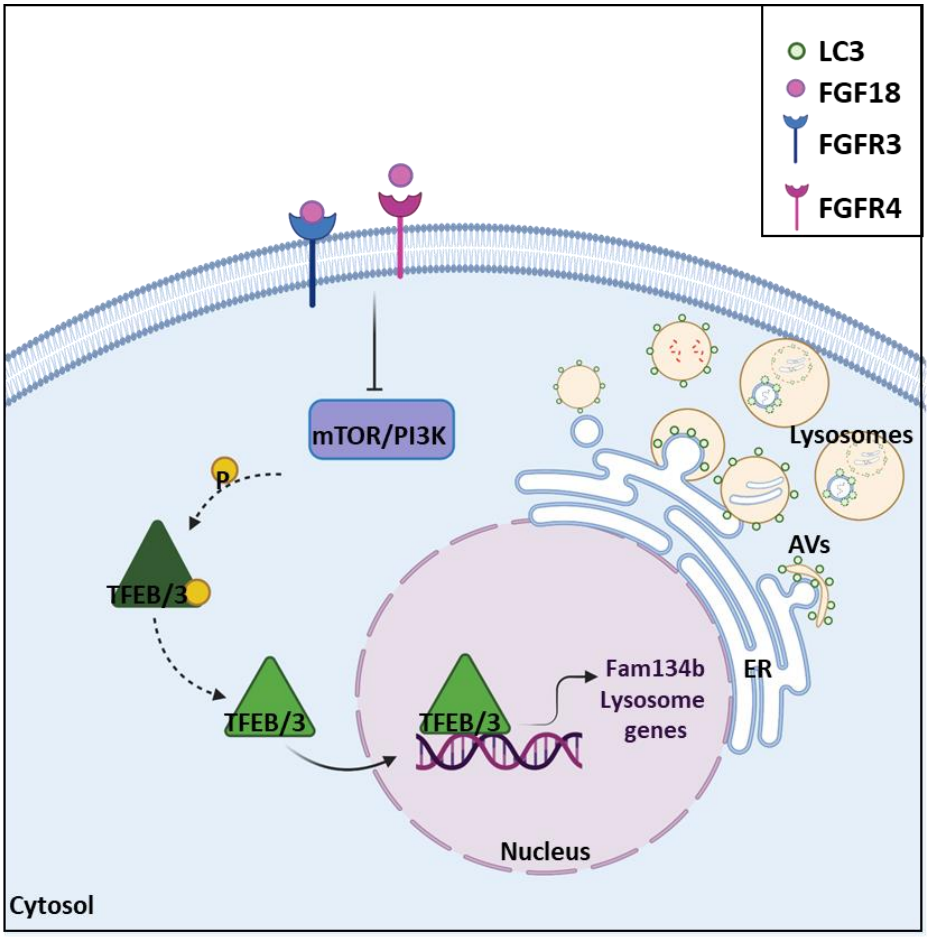

Figure 19. Proposed model of induced ER-phagy in chondrocytes FGF18 through FGFR3 and FGFR4, inhibits the PI3K pathway and promotes TFEB/TFE3 nuclear translocation. In the nucleus, the active transcription factors co-induce the expression of lysosomal, autophagy genes and ER-phagy receptor *Fam134b*.

Using different omic-based approaches (quantitative proteomic, phospho-proteomic, and RNA sequencing), we identified the molecular players through which FGF18 triggers lysosomal degradation of the ER via ER-phagy. Specifically, we found that FGF stimulation promotes cellular catabolism inducing the TFEB/TFE3-dependent enhancement of lysosome biogenesis and the transcriptional induction of *FAM134B*. These data suggests

that the metabolic shift from anabolism to catabolism promoted by MiT-TFe transcription factors can participate to chondrocytes homeostasis.

Notably, FGF18 is still able to activate the autophagy flux in chondrocytes lacking both TFEB and TFE3, suggesting that, at least in this context, the main role of TFEB and TFE3 is to confer substrate selectivity to autophagy. Further studies are needed to understand if the ER-phagy is a part of the general autophagy process or it is a tissue specific TFEB/3-dependent pathway in chondrocytes. We hypothesized that TFEB and TFE3, increasing *FAM134B* expression level, could promote FAM134B oligomerization promoting ER fragmentation and incorporation into autophagosome [36]. Notably, a recent work showed the transcriptional induction of *Fam134b*-2 in the liver [21], suggesting that different and hypothetically tissue specific molecular players could participate to the transcriptional regulation of the ER-phagy. The activity of TFEB and TFE3 factors is mostly regulated by phosphorylation on different serine residues mediated by different kinases, such as mTORC1 and AKT. mTORC1 (the Mammalian Target of Rapamycin) is a serine/threonine phosphatidylinositol-3-kinases related kinase (PI3K) and it covers a central role in the regulation of cellular metabolism and organismal growth [51]. By MS-phospho proteomic data we demostrated that FGF stimulation inhibits the insulin/PI3K signalling cascade, thus leading to TFEB activation. This mechanism could suggest another possible explanation for the inhibitory role of FGF during endochondral ossification. The FGF18-FGFR3 axis promotes chondrocytes differentiation by inhibiting cell proliferation [61]. We hypothesize that the lysosomal degradation of ER membranes via ER-phagy can provide essential metabolites and energy to sustain chondrocyte hypertrophic differentiation. Moreover, we found that the secretion of many differentiation markers is decreased in cells lacking FAM134B, suggesting that the ER-phagy is needed to sustain chondrocytes homeostasis and general protein secretion. Our laboratory recently demonstrated that the FAM134B receptor is also fundamental for the removal of misfolded procollagen from the ER via ER-phagy [4]. Collagen is the most abundant protein secreted by chondrocytes during differentiation. Thus, the activation of the ER-phagy could also participate to the ER-quality control of the cell, removing the misfolded collagen aggregated into the ER lumen and sustaining chondrocytes homeostasis. Notably, FAM134B-mediated lysosomal degradation of the ER was shown to mediate the clearance of other proteins aggregated into the ER lumen, such as alpha1-anti trypsin Z [70].

A detailed overview of the major discussion points will be given in the paragraphs below.

FGF mediate ER-phagy might promote chondrocytes differentiation

Fibroblast growth factors (FGFs) are signalling molecules essential for the regulation of endochondral bone growth, in which cartilage is converted into bone. Cartilage is formed by condensation of mesenchymal cells, which subsequently differentiate into growth plate chondrocytes localized at the ends of the growing bone. Growth plate chondrocytes are arranged in columns that sequentially develop through proliferative, prehypertrophic, and hypertrophic stages [58]. Round proliferative chondrocytes synthesize type II collagen (Col2) and form a columnar layer; they then stop proliferating and become pre-hypertrophic chondrocytes that differentiate into post-mitotic hypertrophic cells. Hypertrophic chondrocytes express predominantly type X collagen (ColX) and mineralize the surrounding matrix [57]. FGF18 might promotes RCS differentiation, in fact upon FGF stimulation they overexpress VEGFA, MMP13, ColX, that are typical hypertrophic chondrocyte markers as assed by qRT-PCR analysis in RCS treated cells (Figure 20).

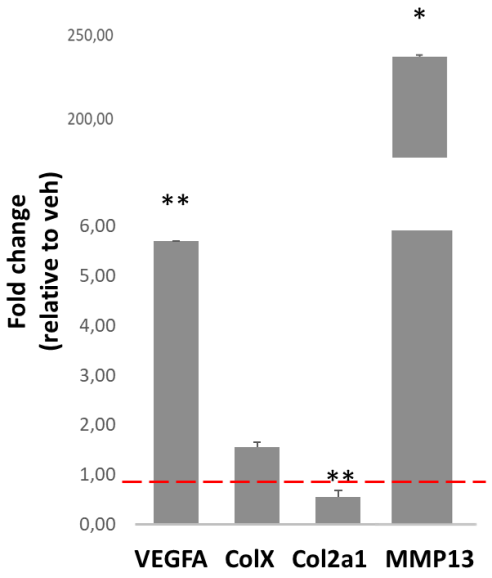

Figure 20. FGF18 might promote chondrocytes differentiation qRT–PCR analysis of hypertrophic chondrocyte markers in RCS. Gene expression was analysed after FGF18 (50ng/ml) treatment for 16h. Fold change values were relative to vehicle (5% ABS) and normalized to Cyclophilin gene. Mean ± standard error of the mean (SEM) of N=3 biological replicates/treatment. Student's paired t-test **P<0.005; *P<0.05.

Therefore, we postulated that ER-phagy could be an essential process induced by FGF18 in chondrocytes to promote the remodelling of the ER *cisternae* to accommodate the replacement of the type II collagen, expressed by pre-hypertrophic chondrocytes, with type X collagen, marker of hypertrophic chondrocytes. Thus, ER remodelling through ER-phagy might be important to promote protein secretion in chondrocytes, particularly during chondrocyte hypertrophic differentiation.

Furthermore, the ER-phagy process could provide to chondrocytes energy and metabolites from the degradation of intracellular membranes and this could be extremely

important to sustain chondrocytes metabolism during differentiation, mostly because the growth plate is a poorly vascularized tissue and chondrocytes are in a state of scarcity of nutrients [65].

FAM134B mediated ER-phagy promotes misfolded collagen clearance

Recent data indicate that FAM134B-mediated ER-phagy is also involved in the clearance of ER luminal misfolded proteins, such as the procollagens (PCs) [4]. Collagens are the most abundant proteins in animals: type I and type II PC (PC1 and PC2) are the major protein components of bone and cartilage, respectively. They are synthesized as single polypeptide chains and folded into triple-helices in the ER [66]. However, approximately 20% of newly synthesized PC1 has been shown to be degraded by lysosomes because of inefficient PC1 folding or secretion and this fraction significantly increases in cases of PC1 mutations [67-68]. Similarly, a fraction of PC2 produced by chondrocytes of the growth plate is degraded by autophagy. Mechanistically, the delivery of PCs into autophagosomes is driven, at least in part, by FAM134B mediated ER-phagy. FAM134B forms a complex with the ER-resident chaperone calnexin (CANX), which acts as a co-receptor, for the selective removal of misfolded PC cargoes. Indeed, FAM134B lacks an ER luminal domain, thus a selective interaction with PCs appears to be mediated by CANX [4]. A recent study has identified the involvement of FAM134B in the quality control of the NPC intracellular cholesterol transporter 1 (NPC1) [69]. NPC1 mediates intracellular cholesterol trafficking in mammals and when mutated causes Niemann-Pick type C disease, a fatal and progressive neurodegenerative disorder characterized by intracellular accumulation of unesterified cholesterol. The NPC1 mutant has been described to accumulate in the ER lumen and to be degraded by two independent pathways functioning in a complementary fashion. It is degraded in part by ER-phagy, in a FAM134B and autophagy-dependent process, and also it is triaged through ERAD by the proteasome via MARCH6, an E3 ubiquitin ligase involved in the control of cholesterol homoeostasis [69]. Thus, the identification of the mechanisms controlling ER-phagy might be exploited for the treatment of protein conformational disease ER such as alpha1-antitrypsin Z mutant and collagens [4;70].

TFEB/TFE3 could promote bulk and different selective autophagy

In vivo studies have shown that TFEB/3 control the expression of genes involved in different energy metabolic pathways in a tissue-specific manner, suggesting that the lysosome/autophagy pathway might be co-regulated with different, organ specific, metabolic programs such as lipid catabolism in liver and carbohydrate metabolism in muscles [71;72]. In chondrocytes, but not in other cell types, we demonstrated that FGF signalling controls ER-phagy transcriptionally and this is important to maintain cellular

homeostasis, suggesting a tissue-specific regulation and function of autophagy. Hence, autophagy *in vivo* might have cargo selectivity that depends on the composition and function of the tissue analysed. Future studies will be focused on the analysis of the autophagy selectivity *in vivo* in different tissues and to the dissection of underlying regulatory mechanisms. Preliminary data showed by qRT-PCR that TFEB enhances the expression of different selective autophagy receptors in a cell specific fashion (data not shown) and most importantly microarray analysis of liver and muscle in mice showed the transcriptional induction of diverse selective autophagy receptors upon TFEB overexpression (Table 2).

Our work has the potential to elucidate new molecular mechanisms controlling substrates recognition and selectivity during autophagy.

Table 2. Microarray analysis from TFEB overexpressing (OE) mice.

SAR (Selective Autophagy Receptors)	TFEB LIVER - OE (GSE35015)	TFEB MUSCLE - OE (GSE62975)
NBR1	up	-
TAX1BP1	up	-
NIX	-	-
BNIP3	-	down
FUNDC1	-	down
PHB2	-	up
NBR1	up	-
TRIM16	-	-
FAM134B	-	up
SEC62	down	down
RTN3	up	up
TEX264	up	-

Concluding Remarks

The FAM134B-mediated ER-phagy plays different and fundamental cellular functions, from maintaining ER homeostasis and size to the selective removal of specific cargoes from the ER. The discovery of the cellular mechanisms governing ER-phagy highlighted the potential therapeutic relevance: enhancing *FAM134B* expression level via TFEB, for instance, could promote the ER-phagy process to sustain the cell health and fitness.

Materials and Methods

Cell culture, transfections, and plasmids

RCS cell line was a Swarm chondrosarcoma chondrocyte line (King & Kimura, 2003). RCS were cultured in DMEM (Euroclone), supplemented with 10% fetal bovine serum (FBS from Euroclone) and 1% P/S. In FGF18 experiments, cells were cultured in DMEM supplemented with 5% adult bovine serum (ABS from Bio-Techne) (vehicle). For transfection experiments, cells were transfected with Lipofectamine LTX and Plus reagent (Invitrogen) following reverse transfection protocol according to the manufacturer's instructions.

Plasmids

TFEB, PRK5-TFE3, and Myc-MITF were described (Anet al, 2019); CMV-Runx2 was a gift from G. Karsenty (Columbia University, New York); FOXO3-HA was a gift from R. Polishchuck (TIGEM, Italy); Pgl3basic luciferase plasmids were from Addgene. eGFP-mCherry-Ramp4 plasmid was a gift from E. Corn (Berkeley, California). TFEB S142A:S211-GFP TFE3 S246A:S312A-GFP, and eGFP-mCherry-LC3 plasmids were previously described (Settembre et al,2011; Di Malta et al., 2017). FAM134B1-HA expression plasmid was described (Khanimetset al, 2015) and FAM13B2-HA was produced by cloning strategy.

Generation of CRISPR clones

Disruption of genes of interest was obtained through clustered regularly interspaced short palindromic repeats (CRISPR)/CRISPR-associated protein 9 (Cas9) technology. 1×10^6 RCS chondrocytes were transfected with 5µg of all-in-one vector containing the sgRNA of interest:

FGFR1 sgRNA sequence: GCATCGTGGAGAACGAGTATGG;
FGFR2 sgRNA sequence: TTTCGGTGTTGGTCCAGTACGG;
FGFR3 sgRNA sequence: ACGCGGGTGTCCTCAGCTACGG;
FGFR4 sgRNA sequence: TCCACGGAGAGAATCGTATCGG;
TFEB sgRNA sequence: GCTGCCATGGCGTCGCGCATCGG;
TFE3 sgRNA sequence: AGTCGTCCACCCCCTGCTC;
Fam134b sgRNA sequence: TGAGCTCTGTGGGTAAGCCAAGG;
ATG9A sgRNA sequence: CTCGTCCCGGGTCTGCGAGCGG;
Gusb sgRNA sequence: CTTCGCGGGAACTCAAGGTG;
Beclin1 sgRNA sequence: GTTTTCTGCCACCACCTTT;
ATG7 sgRNA sequence: CGCTGAGGTTCACCATCCT;

The all-in one vector contains the U6 promoter, a recombinant form of Cas9 protein under the control of CMV promoter, and a eGFP or mCherry reporter gene under the control of the SV40promoter (Sigma-Aldrich). Forty-eight hours after transfection, putative clones

were FACS sorted for the eGFP or mCherry fluorescence using the BD FACS Aria. Sorted cells were kept in culture until confluence and then subject to PCR analysis followed by Sanger sequencing to identify mutations. Selected clones were validated by Western blotting analysis of protein of interest.

Transmission electron microscopy

For routine EM analysis, the cells were fixed with 1% glutaraldehyde (GA) prepared in 0.2 M HEPES buffer (pH 7.4) for 30 min at room temperature (RT). Mouse growth plates (P8) were fixed using a mixture of 2%paraformaldehyde (PFA) and 1% GA prepared in 0.2 M HEPES buffer for 24 h at 4°C. For immuno-EM analysis, the cells were fixed with a mixture of 4% PFA and 0.05% GA for 10 min at RT, then washed with 4% PFA once to remove the residual GA, and fixed again with 4% PFA for 30 min at RT. Next, the cells were incubated with a blocking/permeabilizing mixture (0.5%BSA, 0.1% saponin, 50 mM NH_4Cl) for 30 min and subsequently with the primary polyclonal antibody against GFP (Abcam, Cat No. AB 290-50) diluted 1:250 in blocking/permeabilizing solution. The following day, the cells were washed and incubated with the secondary antibody, the anti-rabbit Fab fragment coupled to 1.4 nm gold particles (Nanoprobes, Cat No2004, anti-rabbit nanogold) diluted 1:50 in blocking/permeabilizing solution for 2 h at RT. All specimens were then post-fixed as described in Polishchuk and Polishchuk (2019). After dehydration, the specimens were embedded in epoxy resin and polymerized at 60°C for 72 h. Thin60-nm sections were cut on a Leica EM UC7 microtome. EM images were acquired from thin sections using a FEI Tecnai-12electron microscope equipped with a VELETTA CCD digital camera (FEI, Eindhoven, The Netherlands). Morphometric analysis on the size of lysosomes was performed using ITEM software (Olympus SYS, Germany).

EATR assay

1×10^6 RCS were transfected with 4µg of eGFP-mCherry-RAMP4, and the expression of the plasmid was induced with doxycycline (Sigma-Aldrich) 4µg/ml for 48 h. The day before, cells were treated with vehicle and FGF18 50 ng/ml for 16 h or with indicated treatments (BafA1 for 3h 200 nM and actinomycin for 4 h at 1µg/ml). Cells were collected in PBS, and the fluorescence was analysed with BD FACS Aria

GFP-mCherry-LC3 assay

1.5×10^6RCS were transfected with 1µg of eGFP-mCherry-LC3, and the expression of the plasmid was induced for 48 h. The day before, chondrocytes were treated with vehicle and FGF18 50 ng/ml for 16 h or with indicated treatments (BafA1 for 3 h 200 nM). Cells were collected in PBS, and the fluorescence was analysed with BD FACS Aria.

Western blotting

RCS chondrocytes were washed twice with PBS and then scraped in RIPA lysis buffer (20 mM Tris [pH 8.0], 150 mM NaCl, 0.1% SDS, 1% NP-40, 0.5% sodium deoxycholate) supplemented with PhosSTOP and EDTA-free protease inhibitor tablets 1× final concentration (Roche, Indianapolis, IN, USA). Cell lysates were incubated on ice for 20 min; then, the soluble fraction was isolated by centrifugation at 18,000 g for 20 min at 4°C. Total protein concentration in cellular extracts was measured using the colorimetric BCA protein assay kit (Pierce Chemical Co, Boston, MA, USA). Protein extracts, separated by SDS–PAGE and transferred onto PVDF, were probed with primary antibodies overnight against: phospho-P70S6K (Cell Signaling Technology 9234S 1:1,000), P70S6K (Cell Signaling Technology 9202S 1:1,000), phospho-AKT (Cell Signaling Technology 4056 (T308) - 4060 (S473) 1:1,000), AKT (Cell Signaling Technology 9272 1:1,000), B-actin (Novus Biologicals NB600-501 1:5,000), Fam134b (Sigma-Aldrich HPA012077 1:1,000), TFE3 (Sigma-AldrichHPA023881 1:1,000). Transfected human TFEB was detected with human specific TFEB antibody (Cell Signaling Technology BL12896_151:1,000). b-tubulin (Sigma T8660 1:10,000), Lamp1 (Abcam ab24170 1:1,000), LC3 (Novus Biologicals NB100-2220 1:1,000), and Filamin A (Cell Signaling Technology 47621:1,000). Proteins of interest were detected with HRP-conjugated goat anti-mouse or anti-rabbit IgG antibody (1:2000, Vector Laboratories) and visualized with the ECL Star Enhanced Chemiluminescent Substrate (Euroclone) according to the manufacturer's protocol. The Western blotting images were acquired using the Chemi Doc-lt imaging system (UVP).

Lysosomal enzymatic activity

Activity of lysosomal enzyme of interest (b-glucuronidase and b-hexosaminidase) was measured as previously described (Bartolomeo et al, 2017). Briefly, cells were lysed in extraction buffer (50 mM $NaHPO_4$ pH 7.0, 10 mM 2-mercaptoethanol, 10 mM Na_2EDTA, 0.1% sodium lauryl sarcosine, 0.1% Triton X-100) and protein concentration was measured using the colorimetric BCA protein assay kit (Pierce Chemical). 200µg of proteins was incubated with 200 µl of fluorogenic substrate (4-methylumbelliferyl-b-D-glucuronide 2 mM Sigma-Aldrich). For b-glucuronidase; 4-methylumbelliferyl-N-acetyl-b-D-glucosami-nide 6 mM Sigma-Aldrich forb-hexosaminidase) for 1 h at 37°C. The reaction was stopped by adding 200 µl of the carbonate stop buffer (0.5 M $NaHCO_3$/0.5 M Na_2CO_3 pH 7.0), and the fluorescence was measured in a fluorimeter (GloMax-Multi Detection System, Promega) using 365 nm excitation and 460 emission.

LysoTracker and DQ-BSA experiments

LysoTracker DND99 (L7528 Thermo Fisher) was incubated at 50 nM in dark for 40 min at 37°C. Cells were washed three times with PBS 1× and collected; the fluorescence was analysed by FACS Accuri C6; and 10,000 events were collected. DQ Green BSA (D12050

Thermo Fisher) was incubated at 10µg/ml in dark for 15 min at 37°C. Cells were washed three times with PBS 1× and collected; the fluorescence was analysed by FACS Accuri C6; and 10,000 events were collected.

qRT–PCR

RCS cells were harvested for RNA extraction using RNeasy Mini Kit (Cat No./ID: 74106 (250), Qiagen) according to the manufacturer's protocol. 1µg of total RNA was used for reverse-transcription using QuantiTect Reverse Transcription Kit (Qiagen) according to the manufacturer's instructions. qRT–PCR was performed in triplicate using LightCycler 480 SYBER Green I Master (Roche) and analysed by LightCycler 480 (Roche). The Ct valueswere normalized to Cyclophillin or Hprt gene, and the expression of each gene was represented as 2(ΔddCt) relative to control. Primers used were as follows:

CtsA: Fw5'-CTTGGCTGTACTGGTCATGC-3';Rev50-GGCAAAGTAGACCAGGGAGT-3'
CtsD: Fw5'-GTGGCTTCATGGGGATGGAC-3';Rev5'-GGAGCAAGTTGAGTGTGGCA-3'
Lamp1: Fw5'-AACCCCAGTGTGTCCAAGTA-3';Rev5'-GCTGACAAAGATGTGCTCCT-3'
Mcoln1: Fw5'-GTGAGCTCCAGGCCTACATTG-3';Rev5'-GCCACTTCCACGACGGAA-3'
Fam134a: Fw5'-CAGAACAGCAGGGTCCCATA-3';Rev5'-TCCACTTTAGACCCTGGCTG-3'
Fam134b: Fw5'-ACCCACAGAGCTCAAGACAA-3';Rev5'-CTGGTCTTTGATGGCAGCTG-3';
Fam134c: Fw5'-CCCAGTCTTGTCCCCTGAAT-3';Rev5'-TTGCCTGTAGTACCACCCTG-3'
Sec62: Fw5'-TCTGGCCAGCAGAAATGAGA-3';Rev5'-CAGTCAGGTTTGGCAGGAAC-3'
Atl3: Fw5'-ACCCCTGCAGTTCTGTTCAC-3';Rev5'-CCCAGCTCAAGATACTGCCC-3'
Rtn3: Fw5'-TCTCACACACTACAGCAGCA-3';Rev5'- TGAGCGATGTTCACTCCTGT-3'
Ccpg1: Fw5'-TCTTGTGGCTGGACTGTCAT-3';Rev5'-TTTGCACTGCTTTCTCCACC-3'
Tex264: Fw5'-GTGCCAGAGGTGAAGGAGAC-3';Rev5'-TTGCTTGCCCCAGGAGAAAA-30
Fam134b-2: Fw5'-ACAGGAGGCAGTCACTTTGG-3'Rv5'-TGCTTGCCACAACTCAGACA-3'
Fam134b-1: Fw5'-CTACGGAGGAGCAGGAACC-3'Rv5'-GGCCTCTTCCAGCTCAGG-3'

Mouse growth plates were lysate by tissue lyser (Qiagen) in 1 ml of TRIzol (Invitrogen) buffer for RNA extraction. RNA was isolated by chloroform phase separation and precipitated using isopropylalcohol. RNA was eluted in RNase-free water. 1µg of total RNA was used for reverse transcription using QuantiTect Reverse Transcription Kit (Qiagen) according to the manufacturer's instructions. qRT–PCR was performed in triplicate using LightCycler 480 SYBER Green I Master (Roche) and analysed by LightCycler 480 (Roche). The Ct values were normalized to Hprtgene, and the expression of each gene was represented as 2ΔddCt relative to control. Primers used were as follows:

Fam134b-2 Fw5'-CATAATAGTCCACTCCTCGGCTTC-3'Rv5'- CTCAGTCTGGCTCTTTCATCTG-3

QuantSeq 3' mRNA sequencing library preparation

RCS chondrocytes wild type and CRISPR-KO for the FGF receptors FGFR3 and FGFR4 (3 biological replicates/condition) were overnight cultured in 5% ABS with or without FGF18. Total RNA was extracted according to the manufacturer's instructions (RNeasy Mini Kit, CatNo. /ID: 74106 (250), Qiagen); RNA extracted from both cell lines untreated was used as control. RNA extracted was quantified and mixed at 50 ng/5µl. Total RNA (100 ng) from each sample was prepared using QuantSeq 30mRNA-Seq Library prep kit (Lexogen, Vienna, Austria) according to the manufacturer's instructions. The amplified fragments of cDNA (300 bp long) were sequenced in single-end mode using the NextSeq 500 (Illumina) with a read length of 75 bp.

QuantSeq3'mRNA sequencing data processing and analysis

Sequence reads were trimmed using Trim Galore software () to remove adapter sequences and low-quality end bases and the naligned on rn6 reference sequence using STAR (Dobin et al, 2013). The expression levels of genes were determined with ht seq-count (Anders et al, 2015) using the Gencode v19 gene model (Harrow et al, 2012). The data have been deposited in NCBIs Gene Expression Omnibus (GEO) and are accessible through GEO Series accession number GSE120516. Differential expression analysis was performed using edgeR (Robinson et al, 2010), a statistical package based on generalized linear models, suitable for multifactorial experiments. The threshold for statistical significance chosen was false discovery rate (FDR)<0.05: In detail, 2,225 genes were differentially expressed (1,164 genes induced and 1,061 inhibited) in the RCS-FGF18 dataset, while no one was found in the KO-RCS-FGF18 dataset (GSE120516). Gene Ontology Enrichment Analysis (GOEA) was then performed on these two lists by using the DAVID online tool (DAVID Bioinformatics Resources 6.8) restricting the output to biological process terms (BP_FAT), cellular compartment terms (CC_FAT), and molecular function terms (MF_FAT). The Kyoto Encyclopedia of Genes and Genomes (KEGG Pathway) analysis was also performed. The threshold for statistical significance of GOEA was FDR<0.1 and enrichmentscore≥1.5, while for the KEGG Pathway analysis was FDR<0.1.

MS-proteomics and phospho-proteomics

Cells were lysed in SDC lysis buffer containing 4% (w/v) SDC,100 mM Tris–HCl (pH 8.5). Proteome preparation was done using the in StageTip (iST) method (Kulak et al, 2014). Phosphopeptides were enriched using the EasyPhos workflow (Humphrey et al,2015). Peptides were desalted on STAGE tips and separated on a reverse-phase column (50 cm, packed in-house with 1.9-lm C18-Reprosil-AQ Pur reversed-phase beads) (Dr Maisch GmbH) over120 min single-run gradients at a flow rate of 350 nl on an EASY-nLC 1200 system (Thermo Fisher Scientific) and analysed by electrospray tandem mass

spectrometry on a QExactive HFX (ThermoFisher Scientific) using HCD-based fragmentation. MS data were acquired using a data-dependent top-15 method with maximum injection time of 20 ms, a scan range of 300–1650Th, and an AGC target of 3e6. Survey scans were acquired at a resolution of 60,000. Resolution for HCD spectra was set to 15,000 with maximum ion injection time of 28 ms and an under fill ratio of either 30%. Dynamic exclusion was set to 20s. Phosphopeptides were eluted with a 140 min gradient. The maximum injection time was 20 ms, at a scan range of 300–1650 Th and an AGC target of 3e6. Sequencing was performed via higher energy collisional dissociation fragmentation with a target value of 1e5 and a window of 1.6Th. Surveyscans were acquired at a resolution of 60,000. Resolution for HCD spectra was set to 15,000 with a maximum ion injection time of120 ms and an underfill ratio of 40%. Dynamic exclusion was set to40s, and apex trigger (4–7s) was enabled.

MS data processing and analysis

Raw mass spectrometry data were processed with Max Quantversion 1.5.5.2 using default settings (FDR 0.01, oxidized methionine (M) and acetylation (protein N-term) as variable modifications, and carbamidomethyl (C) as fixed modification). Label-free quantitation (LFQ) and "Match between runs" were enabled. For phospho-proteomic analysis, phospho-STY was used as a variable modifi-cation. Bioinformatics analysis was performed with Perseus 1.5.4.2. Annotations were extracted from UniProtKB, Gene Ontology (GO),and the Kyoto Encyclopedia of Genes and Genomes (KEGG).The mass spectrometry proteomics data have been deposited to the Proteome Xchange Consortium via the PRIDE (Perez-Riverol et al, 2019) partner repository with the dataset identifier PXD015326(RCS-FGF18/FAM134BKO-FGF18 dataset) and PXD015331 (RCS-FGF18/FGFR3-4KO-FGF18 datasets).

Tandem mass tag secretome

Protein enrichment from cell culture supernatant was done as described before (Bonn & Otto, 2018) with minor modifications. In brief, proteins from 1 ml cell culture supernatant were bound to 20µl primed Strata Clean bead slurry by overnight incubation. Beads were washed with PBS and the proteins denatured by boiling in 2% sodium deoxycholate, 10 mM TCEP, 40 mM, chloroacetamide, and 50 mM Tris, pH 8. Samples were diluted to 1% sodium deoxycholate and digested for 6 h at 37°C with 0.5µg trypsin; after 3 h another 0.5µg trypsin was added. Tryptic peptides were enriched and desalted with SDB-RPS stagetips as described in the IST protocol (Kulak et al, 2014). Peptides were separated by a 63-min non-linear gradient from 5 to 48% acetonitrile on a 20 cm self-packed C18 column with a EASY-nLC 1200 and online injected into a QExactive HF (ThermoFisher). The mass spectrometer was operated in data-dependent mode; after a survey scan with a

resolution of 60,000, the 15 most abundant ions were subjected to HCD fragmentation and analysed with a resolution of 15,000.

Tandem mass tag secretome analysis

Data analysis was done with MaxQuant 1.6.1 with standard parameters and activated LFQ quantification. Differentially abundant proteins were detected by 5% FDR-corrected t-tests performed with Perseus 1.6.2.2. The mass spectrometry proteomics data have been deposited to the Proteome Xchange Consortium via the PRIDE (Perez-Riverol et al, 2019) partner repository with the dataset identifier PXD015130.

Chromatin immunoprecipitation (ChIP)

12×10^6 cells were transfected with pCMV-3×FLAG TFEB-WT for 48 h and treated with FGF18 overnight. Crosslinking was performed for 15 min at RT with 1% formaldehyde in PBS 1x. Formaldehyde quencing was for 5 min with 0.25 M glycine in PBS; cells were scraped on ice with cold PBS and centrifuged at 1000 g 5 min at 4°C; finally, cell lysis was performed on ice for 20 min in ChIP-Lysis buffer (50 mM Tris–HCl, pH 8, 100 mM NaCl, 1% Triton X-100, 1% Tween-20). Chromatin shearing was performed by MNAse digestion (2 U, Sigma-Aldrich) at 37°C for 12 min. Enzymatic reaction was stopped with stop mix buffer (1% sodium dodecyl sulfate (SDS) and 2 mM ethylenedi-aminetetraacetic acid (EDTA)). Unbound SDS was precipitated with SDS-OUT buffer (Pierce, Rockford, IL, USA). Lysates were diluted 1:1with ChIP buffer (50 mM Tris–HCl, pH 8, 100 mM NaCl, 0.25% Triton X-100, 2 mM EDTA) and precleared with High Capacity NeutrAvidinAgarose Resin (Pierce). Protein–DNA complexes were immunoprecipitated with 5ug of ANTI-FLAG BioM2 (Sigma-Aldrich antibody) overnight. Samples were washed three times with ChIP wash buffer (50 mM Tris–HCl, pH 8, 150 mM NaCl, 0.5% Triton X-100, 1 mM EDTA) and twice with ChIP final wash buffer (50 mM Tris–HCl, pH 8,200 mM NaCl, 1 mM EDTA). DNA was eluted by the addition of 8 mM biotin and 1% SDS in ChIP final wash buffer. Upon crosslink reversal, DNA was precipitated overnight with 200 mM NaCl at 65°C, and purification was performed by ChIP DNA Clean &Concentrator (Zymo Research). 1µl of DNA/qPCR was used. Primer sequences used for qPCR were as follows:

MCOLN1: FW5'-CGTCAAGCTTGTCACGTGTTC-3'RV5'-GCGCACCGCGGTCACTG-3'

Fam134b: FW5'-CTTTTGGGTAGAGAAGTGCGTG-3'RV5'-CACAAGCCACAGAACCCATAAT-3'

Luciferase assay

The promoter region of rat Fam134b from 78211858 to 78211187(CLEAR 108404, -2708 from TSS position in intron 3) was amplified by PCR from RCS chondrocyte genome and cloned into pGL3-basic luciferase reporter plasmid (Addgene). 10×10^3cells/treatment were co-transfected with luciferase plasmid and together with 0.2, 0.5, and 1µg of

pLX304-TFEB plasmid. Luciferase assay was performed 48 h after transfection using Dual Luciferase Reporter Assay System (Promega) and normalized for transfection efficiency co-transfecting Renilla luciferase. CLEAR sequence was mutagenized using the Quick Change II mutagenesis kit (Agilent), according to the manufacturer's protocol.

Mice

For histology, femur was fixed overnight in 4% (wt/vol) paraformaldehyde (PFA) and then demineralized in 10% EDTA(pH 7.4) for 48 h. Specimens were embedded in paraffin and sectioned at 7 µm, and stained with hematoxylin and eosin.

Cartilage and bone staining

Staining for cartilage (Alcian Blue) and bone (Alizarin Red) infixed mice was performed according to the standard protocol (http://empress.har.mrc.ac.uk/browser/). Pictures were taken using the DM6000 microscopy (Leica Microsystems, Wetzlar, Germany).

References

1) Ivan Dikic, Zvulun Elazar *Mechanism and medical implications of mammalian autophagy* Nat Rev Mol Cell Biol **19(6):**349-364 (2018).
2) Eleonora Turco, Dorotea Fracchiolla, and Sascha Martens *Recruitment and Activation of the ULK1/Atg1 Kinase Complex in Selective Autophagy* J Mol Biol **432**(1):123-134 (2020).
3) Paolo Grumati, Ivan Dikic, Alexandra Stolz *ER-phagy at a glance* J Cell Sci **131**(17): jcs217364 (2018).
4) Alison Forrester, Chiara De Leonibus, Paolo Grumati, Elisa Fasana, Marilina Piemontese, Leopoldo Staiano, Ilaria Fregno, Andrea Raimondi, Alessandro Marazza, Gemma Bruno, Maria Iavazzo, Daniela Intartaglia, Marta Seczynska, Eelco van Anken, Ivan Conte, Maria Antonietta De Matteis, Ivan Dikic, Maurizio Molinari & Carmine Settembre *A selective ER-phagy exerts procollagen quality control via a Calnexin-FAM134B complex.* EMBO J38: e99847 (2019).
5) Dianne S. Schwarz, Michael D. Blower *The endoplasmic reticulum: structure, function and response to cellular signaling* Cell. Mol. Life Sci. **73**:79–94 (2016).
6) Amber R English, Gia K Voeltz *Endoplasmic reticulum structure and interconnections with other organelles* Cold Spring Harb Perspect Biol 1;5(4):a013227 (2013).
7) Tom Shemesh, Robin W. Klemm, Fabian B. Romano, Songyu Wang, Joshua Vaughan, Xiaowei Zhuang, Hanna Tukachinsky, Michael M. Kozlov, and Tom A. Rapoport *A model for the generation and interconversion of ER morphologies* PNAS **111** (49) E5243-E5251 (2014).
8) Jonathon Nixon-Abell, Christopher J Obara, Aubrey V Weigel, Dong Li, Wesley R Legant, C Shan Xu, H Amalia Pasolli, Kirsten Harvey, Harald F Hess, Eric Betzig, Craig Blackstone, Jennifer Lippincott-Schwartz *Increased spatiotemporal resolution reveals highly dynamic dense tubular matrices in the peripheral ER* Science **28**;354(6311): aaf3928 (2016).
9) Matthew Smith and Simon Wilkinson *ER homeostasis and autophagy* Essays in Biochemistry **61:** 625–635 (2017).
10) Simone Fulda 1, Adrienne M Gorman, Osamu Hori, Afshin Samali *Cellular stress responses: cell survival and cell death* Int J Cell Biol **2010**:214074 (2010).
11) D Allan Drummond, Claus O Wilke *The evolutionary consequences of erroneous protein synthesis* Nat Rev Genet **10**(10):715-24 (2009).

12) Chunyan Xu, Beatrice Bailly-Maitre, and John C. Reed *Endoplasmic reticulum stress: cell life and death decisions* The Journal of Clinical Investigation 10: 2656-2664 (2005).
13) Christopher M Dobson *Getting out of shape* Nature 15;418(6899):729-30 (2002)
14) Navit Ogen-Shtern, Tamuz Ben David, Gerardo Z Lederkremer *Protein aggregation and ER stress* Brain Res 1;**1648**(Pt B):658-666 (2016).
15) Karina Cuanalo-Contreras, Abhisek Mukherjee, Claudio Soto *Role of protein misfolding and proteostasis deficiency in protein misfolding diseases and aging* Int J Cell Biol **2013**:638083 (2013).
16) C De Duve, R Wattiaux *Functions of lysosomes* Annu Rev Physiol **28**:435-92. (1966).
17) Maurizio Molinari *ER-phagy responses in yeast, plants, and mammalian cells and their crosstalk with UPR and ERAD* Dev Cell **56**(7):949-966 (2021).
18) Fulvio Reggiori, Maurizio Molinari *ER-phagy: mechanisms, regulation, and diseases connected to the lysosomal clearance of the endoplasmic reticulum* Physiol Rev **102**(3):1393-1448 (2022).
19) Alessio Reggio, Viviana Buonomo, Rayene Berkane, Ramachandra M Bhaskara, Mariana Tellechea, Ivana Peluso, Elena Polishchuk, Giorgia Di Lorenzo, Carmine Cirillo, Marianna Esposito, Adeela Hussain, Antje K Huebner, Christian A Hübner, Carmine Settembre, Gerhard Hummer, Paolo Grumati, Alexandra Stolz *Role of FAM134 paralogues in endoplasmic reticulum remodeling, ER-phagy, and Collagen quality control* EMBO Rep **22**(9): e52289 (2021
20) Aliaksandr Khaminets, Theresa Heinrich, Muriel Mari, Paolo Grumati, Antje K Huebner, Masato Akutsu, Lutz Liebmann, Alexandra Stolz, Sandor Nietzsche, Nicole Koch, Mario Mauthe, Istvan Katona, Britta Qualmann, Joachim Weis, Fulvio Reggiori, Ingo Kurth, Christian A Hübner, Ivan Dikic *Regulation of endoplasmic reticulum turnover by selective autophagy* Nature **522**(7556):354-8 (2015).
21) Shohei Kohno, Yuji Shiozaki, Audrey L Keenan, Shinobu Miyazaki-Anzai, Makoto Miyazaki *An N-terminal–truncated isoform of FAM134B (FAM134B-2) regulates starvation-induced hepatic selective ER-phagy* Life Sci Alliance **2**(3): e201900340 (2019).
22) Paolo Grumati, Giulio Morozzi, Soraya Holper, Muriel Mari, Marie-Lena IE Harwardt, Riqiang Yan, Stefan Muller, Fulvio Reggiori, Mike Heilemann, Ivan Dikic *Full length RTN3 regulates turnover of tubular endoplasmic reticulum via selective autophagy* eLife **6**:e25555 (2017).

23) Jin Rui Liang, Emily Lingeman, Saba Ahmed, Jacob E Corn *Atlastins remodel the endoplasmic reticulum for selective autophagy* J Cell Biol **217**(10):3354-3367 (2018).

24) Fiorenza Fumagalli, Julia Noack, Timothy J Bergmann, Eduardo Cebollero, Giorgia Brambilla Pisoni, Elisa Fasana, Ilaria Fregno, Carmela Galli, Marisa Loi, Tatiana Soldà, Rocco D'Antuono, Andrea Raimondi, Martin Jung, Armin Melnyk, Stefan Schorr, Anne Schreiber, Luca Simonelli, Luca Varani, Caroline Wilson-Zbinden, Oliver Zerbe, Kay Hofmann, Matthias Peter, Manfredo Quadroni, Richard Zimmermann, Maurizio Molinari *Translocon component Sec62 acts in endoplasmic reticulum turnover during stress recovery* Nat Cell Biol **18**(11):1173-1184 (2016).

25) Matthew D.Smith, Margaret E.Harley, Alain J.Kemp, Jimi Wills, Martin Lee, Mark Arends, Alexvon Kriegsheim,Christian Behrends, Simon Wilkinson *CCPG1 Is a Non-canonical Autophagy Cargo Receptor Essential for ER-Phagy and Pancreatic ER Proteostasis* Developmental Cell **44**(2):217-232 (2018).

26) Heeseon An, Alban Ordureau, Joao A Paulo, Christopher J Shoemaker, Vladimir Denic, J Wade Harper *TEX264 Is an Endoplasmic Reticulum-Resident ATG8-Interacting Protein Critical for ER Remodeling during Nutrient Stress* Mol Cell **74**(5):891-908 (2019).

27) Gia K Voeltz, William A Prinz, Yoko Shibata, Julia M Rist, Tom A Rapoport *A class of membrane proteins shaping the tubular endoplasmic reticulum* Cell **124**(3):573-86 (2006).

28) Junjie Hu, Yoko Shibata, Peng-Peng Zhu, Christiane Voss, Neggy Rismanchi, William A Prinz, Tom A Rapoport, Craig Blackstone *A class of dynamin-like GTPases involved in the generation of the tubular ER network* Cell **138**(3):549-61 (2009).

29) Haruka Chino, Tomohisa Hatta, Tohru Natsume, Noboru Mizushima *Intrinsically Disordered Protein TEX264 Mediates ER-phagy* Mol Cell **74**(5):909-921 (2019).

30) Francescopaolo Iavarone, Giorgia Di Lorenzo, Carmine Settembre *Regulatory events controlling ER-phagy* Curr Opin Cell Biol **76**:102084 (2022).

31) The GTEx Consortium *The Genotype-Tissue Expression (GTEx) pilot analysis: Multitissue gene regulation in humans* Scienze **348**:648-660 (2015).

32) Dongxue Wang, Basak Eraslan, Thomas Wieland, Björn Hallström, Thomas Hopf, Daniel Paul Zolg, Jana Zecha, Anna Asplund, Li-hua Li, Chen Meng, Martin Frejno, Tobias Schmidt, Karsten Schnatbaum, Mathias Wilhelm, Frederik Ponten, Mathias Uhlen, Julien Gagneur, Hannes Hahne, Bernhard Kuster *A deep proteome and*

transcriptome abundance atlas of 29 healthy human tissues Molecular Systems Biology **15**:e8503 (2019).

33) Wing K Tang, Chung H Chui, Sarwat Fatima, Stanton H L Kok, Kai C Pak, Tian M Ou, Kin S Hui, Mei M Wong, John Wong, Simon Law, S W Tsao, King Y Lam, Philip S L Beh, Gopesh Srivastava, Albert S C Chan, Kwok P Ho, Johnny C O Tang *Oncogenic properties of a novel gene JK-1 located in chromosome 5p and its overexpression in human esophageal squamous cell carcinoma*. Int J Mol Med 19:915–923 (2007).
34) Kais Kasem, Emily Sullivan, Vinod Gopalan, Ali Salajegheh, Robert A Smith, Alfred K-Y Lam *JK1 (FAM134B) represses cell migration in colon cancer: a functional study of a novel gene* Exp Mol Pathol **97**(1):99-104 (2014).
35) Ingo Kurth, Torsten Pamminger, J Christopher Hennings, Désirée Soehendra, Antje K Huebner, Annelies Rotthier, Jonathan Baets, Jan Senderek, Haluk Topaloglu, Sandra A Farrell, Gudrun Nürnberg, Peter Nürnberg, Peter De Jonghe, Andreas Gal, Christoph Kaether, Vincent Timmerman, Christian A Hübner *Mutations in FAM134B, encoding a newly identified Golgi protein, cause severe sensory and autonomic neuropathy* Nat Genet 41(11):1179-81 (2009).
36) Ramachandra M Bhaskara, Paolo Grumati, Javier Garcia-Pardo, Sissy Kalayil, Adriana Covarrubias-Pinto, Wenbo Chen, Mikhail Kudryashev, Ivan Dikic, Gerhard Hummer *Curvature induction and membrane remodeling by FAM134B reticulon homology domain assist selective ER-phagy* Nat Commun **10**(1):2370 (2019).
37) Umur Keles, Evin Iscan, Huriye Erbak Yilmaz, Gökhan Karakülah, Aslı Suner, Erhan Bal, Nilgun Tasdemir, Ayse Derya Cavga, Umut Ekin, Zeynep Mutlu, Sila Kahyaoglu, Muhittin A. Serdar, Nese Atabey, and Mehmet Ozturk *Differential expression of full-length and NH2 terminally truncated FAM134B isoforms in normal physiology and cancer* Am J Physiol Gastrointest Liver Physiol **319**: G733–G747 (2020).
38) 7. Tian X, Jin RU, Bredemeyer AJ, Oates EJ, Błazewska KM, McKenna CE, et al.: *RAB26 and RAB3D are direct transcriptional targets of MIST1 that regulate exocrine granule maturation.* Mol Cell Biol **30**:1269–1284 (2010).
39) Won JaeHuh**,** Emel Esen, Jessica H.Geahlen, Andrew J.Bredemeyer, Ann Hwee Lee, Guanglu Shi Stephen F.Konieczny Laurie H.Glimcher Jason C.Mills *XBP1 controls maturation of gastric zymogenic cells by induction of MIST1 and expansion of the rough endoplasmic reticulum* Gastroenterology **139**:2038–2049 (2010).
40) Svenja Zielke, Simon Kardo, Laura Zein, Muriel Mari, Adriana Covarrubias-Pinto, Maximilian N Kinzler, Nina Meyer, Alexandra Stolz, Simone Fulda, Fulvio Reggiori,

Donat Kögel, Sjoerd van Wijk *ATF4 links ER stress with reticulophagy in glioblastoma cells* Autophagy **17**(9):2432-2448 (2021).

41) Qiang Zhang, Xilong Zhang, Ning Ding, Luyao Ge, Yanbin Dong, Can He, Wenxiao Ding *Globular adiponectin alleviates chronic intermittent hypoxia-induced H9C2 cardiomyocytes apoptosis via ER-phagy induction* Cell Cycle **19**(22):3140-3153 (2020).
42) Qingzhou Chen, Ya Xiao, Peiyuan Chai, Pengli Zheng, Junlin Teng, Jianguo Chen *ATL3 Is a Tubular ER-Phagy Receptor for GABARAP-Mediated Selective Autophagy* Curr Biol **29**(5):846-855 (2019).
43) Eiríkur Steingrímsson, Neal G Copeland, Nancy A Jenkins *Melanocytes and the microphthalmia transcription factor network* Annu Rev Genet **38**:365-411 (2004).
44) T J Hemesath, E Steingrímsson, G McGill, M J Hansen, J Vaught, C A Hodgkinson, H Arnheiter, N G Copeland, N A Jenkins, D E Fisher *microphthalmia, a critical factor in melanocyte development, defines a discrete transcription factor family* Genes Dev **8**(22):2770-80 (1994).
45) Vivian Pogenberg, Margrét H Ogmundsdóttir, Kristín Bergsteinsdóttir, Alexander Schepsky, Bengt Phung, Viktor Deineko, Morlin Milewski, Eiríkur Steingrímsson, Matthias Wilmanns *Restricted leucine zipper dimerization and specificity of DNA recognition of the melanocyte master regulator MITF Genes* Dev **26**(23):2647-58 (2012).
46) Gennaro Napolitano, Andrea Ballabio *TFEB at a glance* J Cell Sci **129**(13):2475-81 (2016).
47) Carmine Settembre, Alessandro Fraldi, Diego L Medina, Andrea Ballabio *Signals from the lysosome: a control centre for cellular clearance and energy metabolism* Nat Rev Mol Cell Biol **14**(5):283-96 (2013).
48) Marco Sardiello, Michela Palmieri, Alberto di Ronza, Diego Luis Medina, Marta Valenza, Vincenzo Alessandro Gennarino, Chiara Di Malta, Francesca Donaudy, Valerio Embrione, Roman S Polishchuk, Sandro Banfi, Giancarlo Parenti, Elena Cattaneo, Andrea Ballabio *A gene network regulating lysosomal biogenesis and function* Science **325**(5939):473-7 (2009).
49) Michela Palmieri, Soren Impey, Hyojin Kang, Alberto di Ronza, Carl Pelz, Marco Sardiello, Andrea Ballabio *Characterization of the CLEAR network reveals an integrated control of cellular clearance pathways* Hum Mol Genet **20**(19):3852-66 (2011).
50) Carmine Settembre, Chiara Di Malta, Vinicia Assunta Polito, Moises Garcia Arencibia, Francesco Vetrini, Serkan Erdin, Serpil Uckac Erdin, Tuong Huynh, Diego Medina, Pasqualina Colella, Marco Sardiello, David C Rubinsztein, Andrea

Ballabio *TFEB links autophagy to lysosomal biogenesis* Science **332**(6036):1429-33. (2011)

51) Carmine Settembre, Roberto Zoncu, Diego L Medina, Francesco Vetrini, Serkan Erdin, SerpilUckac Erdin, Tuong Huynh, Mathieu Ferron, Gerard Karsenty, Michel C Vellard, Valeria Facchinetti, David M Sabatini, Andrea Ballabio *A lysosome-to-nucleus signalling mechanism senses and regulates the lysosome via mTOR and TFEB* EMBO J **31**(5):1095-108 (2012).
52) Agnes Roczniak-Ferguson, Constance S Petit, Florian Froehlich, Sharon Qian, Jennifer Ky, Brittany Angarola, Tobias C Walther, Shawn M Ferguson *The transcription factor TFEB links mTORC1 signaling to transcriptional control of lysosome homeostasis* Sci Signal **5**(228):ra42 (2012).
53) José A Martina, Heba I Diab, Li Lishu, Lim Jeong-A, Simona Patange, Nina Raben, Rosa Puertollano *The nutrient-responsive transcription factor TFE3 promotes autophagy, lysosomal biogenesis, and clearance of cellular debris* Sci Signal **7**(309):ra9 (2014).
54) Diego L Medina, Simone Di Paola, Ivana Peluso, Andrea Armani, Diego De Stefani, Rossella Venditti, Sandro Montefusco, Anna Scotto-Rosato, Carolina Prezioso, Alison Forrester, Carmine Settembre, Wuyang Wang, Qiong Gao, Haoxing Xu, Marco Sandri, Rosario Rizzuto, Maria Antonietta De Matteis, Andrea Ballabio *Lysosomal calcium signalling regulates autophagy through calcineurin and TFEB* Nat Cell Biol **17**(3):288-99 (2015).
55) Roberto Zoncu, Liron Bar-Peled, Alejo Efeyan, Shuyu Wang, Yasemin Sancak, David M Sabatini *mTORC1 senses lysosomal amino acids through an inside-out mechanism that requires the vacuolar H(+)-ATPase* Science **334**(6056):678-83 (2011).
56) Jose A Martina, Rosa Puertollano *Rag GTPases mediate amino acid-dependent recruitment of TFEB and MITF to lysosomes* J Cell Biol **200**(4):475-91 (2013).
57) Lin-Shu Liu, Chee-Keng Ng, Andrea Y Thompson, James W Poser, Robert C Spiro *Hyaluronate-heparin conjugate gels for the delivery of basic fibroblast growth factor (FGF-2)* J Biomed Mater Res **62**(1):128-35 (2002).
58) David M Ornitz, Pierre J Marie *Fibroblast growth factor signaling in skeletal development and disease* Genes Dev 29(14):1463-86 (2015).
59) Erwin F. Wagner Gerard Karsenty *Genetic control of skeletal development* Current Opinion in Genetics & Development **11**:527–532 (2001).
60) Henry M Kronenberg *Developmental regulation of the growth plate* Nature 423(6937):332-6 (2003).

61) J S Colvin, B A Bohne, G W Harding, D G McEwen, D M Ornitz *Skeletal overgrowth and deafness in mice lacking fibroblast growth factor receptor 3* Nat Genet **12**(4):390-7 (1996).

62) Yingcai Wang, Michal K. Spatz, Karuppiah Kannan, Hovhannisyan Hayk, Aaron Avivi, Marat Gorivodsky, Mark Pines, Avner Yayon, Peter Lonai, and David Givol *A mouse model for achondroplasia produced by targeting fibroblast growth factor receptor 3* Proc. Natl. Acad. Sci. **96:**4455– 4460, (1999).

63) Laura Cinque, Alison Forrester, Rosa Bartolomeo, Maria Svelto, Rossella Venditti, Sandro Montefusco, Elena Polishchuk, Edoardo Nusco, Antonio Rossi, Diego L Medina, Roman Polishchuk, Maria Antonietta De Matteis, Carmine Settembre *FGF signalling regulates bone growth through autophagy* Nature **528**(7581):272-5 (2015).

64) Rosa Bartolomeo, Laura Cinque, Chiara De Leonibus, Alison Forrester, Anna Chiara Salzano, Jlenia Monfregola, Emanuela De Gennaro, Edoardo Nusco, Isabella Azario, Carmela Lanzara, Marta Serafini, Beth Levine, Andrea Ballabio, Carmine Settembre *mTORC1 hyperactivation arrests bone growth in lysosomal storage disorders by suppressing autophagy* J Clin Invest **127**(10):3717-3729 (2017).

65) Yao Q, Khan MP, Merceron C, La Gory EL, Tata Z, Mangiavini L, Hu J, Vemulapalli K, Chandel NS, Giaccia A Jet al *Suppressing mitochondrial respiration is critical for hypoxia tolerance in the fetal growth plate.* Dev Cell **49**:748–763 (2019).

66) Bateman JF, Boot-Handford RP, Lamande´ SR. *Genetic diseases of connective tissues: Cellular and extracellular effects of ECM mutations*. Nat Rev Genet **10**: 173–83 (2009).

67) Yoshihito Ishida, Kazuhiro Nagata *Autophagy eliminates a specific species of misfolded procollagen and plays a protective role in cell survival against ER stress* Autophagy **5**(8):1217-9 (2009).

68) Robert S. Bienkowski, Samantha F. Curran, and Richard A. Berg *Kinetics of intracellular degradation of newly synthesized collagen* Biochemistry **25**(9):2455–2459 (1986).

69) Mark L. Schultz, Kelsey L. Krus, Susmita Kaushik, Derek Dang, Ravi Chopra, Ling Qi, Vikram G. Shakkottai, Ana Maria Cuervo & Andrew P. Lieberman *Coordinate regulation of mutant NPC1 degradation by selective ER autophagy and MARCH6-dependent ERAD* NATURE COMMUNICATIONS **9**:3671 (2018).

70) Ilaria Fregno¸ Elisa Fasana¸ Timothy J Bergmann¸ Andrea Raimondi¸ Marisa Loi¸ Tatiana Soldà¸ Carmela Galli¸ Rocco D'Antuono¸ Diego Morone¸ Alberto Danieli¸

Paolo Paganetti, Eelco van Anken, Maurizio Molinari *ER-to-lysosome-associated degradation of proteasome-resistant ATZ polymers occurs via receptor-mediated vesicular transport* The EMBO Journal **37**:e99259 (2018).

71) Carmine Settembre, Rossella De Cegli, Gelsomina Mansueto, Pradip K Saha, Francesco Vetrini, Orane Visvikis, Tuong Huynh, Annamaria Carissimo, Donna Palmer, Tiemo Jürgen Klisch, Amanda C Wollenberg, Diego Di Bernardo, Lawrence Chan, Javier E Irazoqui, Andrea Ballabio *TFEB controls cellular lipid metabolism through a starvation-induced autoregulatory loop* Nat Cell Biol **15**(6):647-58 (2013).

72) Gelsomina Mansueto, Andrea Armani, Carlo Viscomi, Luca D'Orsi, Rossella De Cegli, Elena V. Polishchuk, Costanza Lamperti, Ivano Di Meo, Vanina Romanello, Silvia Marchet, Pradip K. Saha, Haihong Zong, Bert Blaauw, Francesca Solagna, Caterina Tezze, Paolo Grumati, Paolo Bonaldo, Jeffrey E. Pessin, Massimo Zeviani, Marco Sandri and Andrea Ballabio *Transcription Factor EB Controls Metabolic Flexibility during Exercise* Cell Metab. **25**(1):182-196 (2017).